Multiple Mechanisms Inactivate the LIN-41 RNA-Binding Protein to Ensure A Robust Oocyte-to-Embryo Transition in *Caenorhabditis elegans*

Caroline A. Spike*, Gabriela Huelgas-Morales*, Tatsuya Tsukamoto*, and David Greenstein*,[1]

*Department of Genetics, Cell Biology and Development, University of Minnesota, Minneapolis, Minnesota 55455, USA

Running title: Translational Regulation of Oogenesis

Keywords: oocyte meiotic maturation, the oocyte-to-embryo transition, translational regulation, RNA-binding proteins, ubiquitin-mediated protein degradation

[1]Corresponding author: David Greenstein, Department of Genetics, Cell Biology, and Development, University of Minnesota, 4-208 MCB, 420 Washington Avenue SE, Minneapolis, MN 55455. Tel: 612-624-3955; FAX: 612-626-6140. E-mail: green959@umn.edu

ABSTRACT

In the nematode *Caenorhabditis elegans*, the conserved LIN-41 RNA-binding protein is a translational repressor that coordinately controls oocyte growth and meiotic maturation. LIN-41 exerts these effects, at least in part, by preventing the premature activation of the cyclin-dependent kinase CDK-1. Here we investigate the mechanism by which LIN-41 is rapidly eliminated upon the onset of meiotic maturation. Elimination of LIN-41 requires the activities of CDK-1 and multiple SCF-type ubiquitin ligase subunits, including the conserved substrate adaptor protein SEL-10/Fbw7/Cdc4, suggesting that LIN-41 is a target of ubiquitin-mediated protein degradation. Within the LIN-41 protein, two non-overlapping regions, Deg-A and Deg-B, are individually necessary for LIN-41 degradation; both contain several potential phosphodegron sequences, and at least one of these sites is required for LIN-41 degradation. Finally, Deg-A and Deg-B are sufficient, in combination, to mediate SEL-10-dependent degradation when transplanted into a different oocyte protein. Although LIN-41 is a potent inhibitor of protein translation and M-phase entry, the failure to eliminate LIN-41 from early embryos does not result in the continued translational repression of LIN-41 oocyte mRNA targets. Based on these observations, we propose a molecular model for the elimination of LIN-41 by SCF^{SEL-10} and suggest that LIN-41 is inactivated before it is degraded. Furthermore, we provide evidence that another RNA-binding protein, the GLD-1 tumor suppressor, is regulated similarly. Redundant mechanisms to extinguish translational repression by RNA-binding proteins may both control and provide robustness to irreversible developmental transitions, including meiotic maturation and the oocyte-to-embryo transition.

INTRODUCTION

The genetic pathways controlling developmental decisions have evolved to be robust to perturbations stemming from environmental change, nutrient deprivation, and endogenous genetic variation (reviewed by Hammerstein *et al*. 2005; Félix and Wagner 2008). At a genetic level, robustness stems in large part from redundancy of control and feedback and feed-forward regulatory mechanisms built into the pathways. In turn, redundancy in genetic control also provides a hardy and permissive substrate to support evolutionary change (reviewed by Prince and Pickett 2002; Vavouri *et al*. 2008). Ultimately, the robustness of genetic pathways is central to the preservation of the germline, the immortal cell lineage required for sexual reproduction and perpetuation of a species. Cell fate decisions in the germline fall into two broad classes, those that are plastic and those that represent irreversible all-or-none commitments. For example, in several organisms the differentiated progeny of germline stem cells can dedifferentiate to repopulate the stem cell niche in response to adverse conditions that deplete the stem cell pool (Brawley and Matunis 2004; Kai and Spradling 2004; Nakagawa *et al*. 2007, 2010; Cheng *et al.* 2008; Barroca *et al*. 2009). By contrast, the commitment of an oocyte to complete meiosis and undergo fertilization represents an irrevocable decision. Here we explore the molecular genetic mechanisms controlling the commitment to fertilization during the final stages of oogenesis in the nematode *Caenorhabditis elegans*.

In *C. elegans*, as in many animals, fully grown oocytes are transcriptionally quiescent and depend on a maternal load of protein and messenger RNA to complete their development. As a consequence, the dramatic cell cycle and developmental changes that occur during the

transition from oogenesis to embryogenesis are driven by post-transcriptional mechanisms. Such mechanisms include protein phosphorylation, the elimination of maternally-provided proteins or mRNAs, and the regulation of maternal mRNA translation (reviewed by Verlhac *et al*. 2010; Robertson and Lin 2015; Svoboda *et al*. 2017). The oocyte-to-embryo transition (OET) initiates when oocytes exit meiotic prophase and enter the first meiotic metaphase (MI), a cell cycle and developmental event also known as meiotic resumption or meiotic maturation. The OET completes when zygotic gene transcription begins after fertilization in the early embryo.

Pioneering studies using amphibian oocytes established that oocyte meiotic maturation is initiated by the activation of maturation-promoting factor (MPF), in response to progesterone from the follicle cells (Masui and Markert 1971; reviewed by Masui 2001). The principal components of MPF are the cyclin-dependent kinase Cdk1 catalytic subunit and a cyclin B regulatory subunit (Dunphy *et al*. 1988; Gautier *et al*. 1988, 1990; Lohka *et al.* 1988; reviewed by Nurse 1990). In *Xenopus*, which represents the best-studied system from a biochemical standpoint, MPF activation involves the translation of multiple, apparently redundantly-acting factors, including the cMos protein kinase, B-type cyclins, RINGO/Speedy, and proteins that remain to be identified (Kobayashi *et al*. 1991; Minshull *et al*. 1991; Nebreda *et al*. 1995; Frank-Vaillant *et al*. 1999; Haccard and Jessus 2006a; reviewed by Haccard and Jessus 2006b). Once activated, MPF stimulates multiple positive feedback mechanisms, including the activation of the Greatwall kinase, which phosphorylates and activates the protein phosphatase 2A (PP2A) inhibitor α-endosulfine (Yu *et al*. 2006; Zhao *et al*. 2008; Von Stetina *et al*. 2008; Castilho *et al*. 2009; Mochida *et al*. 2010). The inhibition of PP2A results in the activation of the CDC25 phosphatase, which removes the inhibitory CDK1 phosphorylations at Thr14 and Tyr15

83 catalyzed by the Wee1 or Myt1 kinases (Kornbluth *et al*. 1994; Mueller *et al*. 1995). The initial
84 signal from MPF activation is amplified in a feed-forward mechanism in which active CDK
85 promotes the inactivation of its inhibitors, Wee1 and Myt1 (reviewed by Ferrell 1999a,b), and
86 stimulates its activator, CDC25 (Kumagai and Dunphy 1996). This regulatory mechanism
87 generates the "switch-like" activation of MPF that promotes the rapid and irreversible cell cycle
88 transition from prophase to metaphase (reviewed by O'Farrell *et al*. 2001; Kishimoto 2015).

89 MPF is the master regulator of cell cycle progression during oocyte meiotic maturation
90 in *C. elegans* as in all examined species (Boxem *et al.* 1999; Burrows *et al*. 2006; van der Voet *et*
91 *al*. 2009), yet MPF activation is regulated somewhat differently than in *Xenopus*. For example,
92 although the inhibitory Wee1/Myt1 kinase Wee-1.3 is crucially important for inhibiting MPF
93 activity in immature *C. elegans* oocytes (Burrows *et al*. 2006), an apparent Greatwall homolog is
94 not found in the *C. elegans* genome and α-endosulfine/*ensa-1* is not required for viability or
95 fertility (Kim *et al*. 2012). Likewise, the signal that triggers MPF activation for meiotic
96 maturation in *C. elegans* is not progesterone, but rather the major sperm protein (MSP), an
97 abundant cytoskeletal protein that is released from sperm (Miller *et al*. 2001; Kosinski *et al*.
98 2005). The latter control mechanism, which serves to link meiotic maturation and ovulation to
99 sperm availability, likely evolved in gonochoristic predecessors of facultative hermaphroditic
100 nematode species like *C. elegans*. The rate of meiotic maturation declines substantially as a *C.*
101 *elegans* hermaphrodite utilizes its limited supply of sperm for self-fertilization but rapidly
102 increases upon mating (Kosinki *et al*. 2005). When sperm are absent, as in mutant
103 hermaphrodites that do not produce sperm (e.g., *fog* mutant females), oocytes arrest for
104 prolonged periods and the rate of production and growth of new oocytes declines until

105 insemination (McCarter *et al*. 1999; Wolke *et al*. 2007; Govindan *et al*. 2009). This serves to
106 preserve metabolically costly oocytes when sperm are unavailable for fertilization. Thus, the
107 molecular mechanisms that control MPF activation must be exquisitely fine-tuned for sperm
108 sensing.

109 Another commonality between the *C. elegans* and *Xenopus* systems is that MPF
110 activation depends on translational control mechanisms, though the details differ. In *C. elegans*,
111 large ribonucleoprotein (RNP) complexes containing the tripartite motif (TRIM)-NHL (NCL-1,
112 HT2A, and LIN-41) RNA-binding protein LIN-41 and the tristetraprolin/TIS11-related RNA-
113 binding proteins OMA-1 and OMA-2 (referred to collectively as the OMA proteins) are major
114 downstream targets of MSP signaling (Spike *et al*. 2014a,b; Tsukamoto *et al*. 2017). LIN-41 is the
115 chief determinant of the extended meiotic prophase of *C. elegans* oocytes (Spike *et al*. 2014a).
116 In *lin-41* null mutants, pachytene-stage oocytes cellularize prematurely, activate CDK-1,
117 aberrantly disassemble the synaptonemal complex, and enter M phase precociously, causing
118 sterility (Matsuura *et al*. 2016; Spike *et al*. 2014a; Tocchini *et al*. 2016). CDK-1 activation causes
119 oocytes to prematurely transcribe and express genes that are ordinarily restricted to
120 differentiated cells and expressed after the OET (Allen *et al*. 2014; Spike *et al*. 2014a; Tocchini
121 *et al*. 2014). LIN-41 inhibits CDK-1 activation in part through the 3'-untranslated region (UTR)-
122 mediated translational repression of the CDC-25.3 phosphatase (Spike *et al*. 2014a,b). By
123 contrast, the OMA proteins are redundantly required for CDK-1 activation (Detwiler *et al*.
124 2001). In the absence of the OMA proteins, oocytes fail to undergo meiotic maturation despite
125 the presence of sperm, resulting in sterility (Detwiler *et al*. 2001).

Genetic analysis suggests the OMA proteins promote meiotic maturation by inhibiting the function of LIN-41 in the most proximal oocyte. Two lines of molecular evidence are consistent with the idea that LIN-41 must be inactivated to promote meiotic maturation. First, LIN-41 is degraded upon the onset of meiotic maturation in response to CDK-1 activation (Spike *et al*. 2014a; Figure 1, A and B). Second, LIN-41 is a potent translational repressor, yet several of the mRNAs it associates with and represses are translated and co-expressed with LIN-41 prior to meiotic maturation in the –1 and –2 oocytes (Tsukamoto *et al*. 2017). These mRNAs include those encoding the RNA-binding protein SPN-4, which is required for development of the embryonic germline and the mesendoderm (Gomes *et al*. 2001), and MEG-1, which is a germplasm or P granule component needed for germline development (Leacock and Reinke 2008; Kapelle and Reinke 2011; Wang *et al*. 2014). By contrast, the OMA proteins are required for the translation of *spn-4* and *meg-1* transcripts in proximal oocytes, providing a molecular mechanism by which the OMA proteins might antagonize LIN-41 function (Tsukamoto *et al*. 2017).

Here we examine the mechanism by which LIN-41 is eliminated by the end of the first meiotic division. We identify two LIN-41 degradation domains, Deg-A and Deg-B, and a potential CDK-1 phosphorylation site within Deg-A that are individually required for efficient degradation. Transplantation of both LIN-41 degradation domains into OMA-2 results in the premature degradation of the resulting fusion protein during meiosis. Furthermore, we find that a Skp, Cullin, F-box (SCF) E3 ubiquitin ligase complex containing the substrate recognition subunit SEL-10 promotes the degradation of LIN-41 and likely functions through the newly identified degradation domains of LIN-41. SEL-10 is a highly conserved F-box protein important

for cell-cycle regulation in both yeast (cell division control protein 4 (Cdc4)) and humans (F-box and WD repeat domain protein (FBW7)) (reviewed in Deshaies and Ferrell 2001; Welcker and Clurman 2008).

Intriguingly, we show that SEL-10 is also important for the degradation of the tumor suppressor protein GLD-1/STAR RNA-binding protein, which is required for oocyte differentiation and represses translation in oocytes (Francis *et al*. 1995a,b; Jones and Schedl 1995; Lee and Schedl 2001; Shumacher *et al*. 2005; Wright *et al*. 2011; Jungkamp *et al*. 2011; Scheckel *et al*. 2012; Farley and Ryder 2012; Doh *et al*. 2013). GLD-1 was independently identified as a target of SEL-10-mediated degradation by Kisielnicka *et al*. (2018) along with CPB-3, a cytoplasmic polyadenylation element (CPE)-binding (CPEB) protein, which is also important for oocyte development (Boag *et al*. 2005; Hasegawa *et al*. 2006). GLD-1 and CPB-3 are degraded during meiotic prophase, as immature oocytes transition from pachytene to diplotene (Kisielnicka *et al.* 2018), considerably earlier than the degradation of LIN-41 during the OET. This is likely due to differences in signaling-mediated regulation; while the degradation of LIN-41 is regulated by activated CDK-1 (Spike *et al*. 2014a and this work), the degradation of GLD-1 and CPB-3 is regulated by the MAP kinase MPK-1 (Kisielnicka *et al*. 2018 and this work). Surprisingly, the ectopic expression of LIN-41 and GLD-1 in *sel-10* mutants has only minor effects on fertility and the expression of mRNAs that are translationally repressed by either LIN-41 or GLD-1 during oogenesis. We suggest that the LIN-41 that persists in the embryos of *sel-10* and certain *lin-41* mutants is likely inactivated by additional post-transcriptional mechanisms that remain to be identified.

MATERIALS AND METHODS

Strains

The genotypes of strains used in this study are reported in Table S1. The following mutations were used: LGI – *mex-3(tn1753[gfp::3xflag::mex-3])*, *air-2(or207*ts*)*, *unc-13(e1091)*, *rrf-1(pk1417*), *gld-1(q485)*, *lin-41(tn1487*ts*)*, *lin-41(tn1541[gfp::tev::s-tag::lin-41]*, *lin-41(tn1541tn1548)*, *lin-41(tn1541tn1562)*, *lin-41(tn1541tn1571)*, *lin-41(tn1541tn1618)*, *lin-41(tn1541tn1620)*, *lin-41(tn1541tn1622)*, *lin-41(tn1541tn1628)*, *lin-41(tn1541tn1630)*, *lin-41(tn1541tn1635)*, *lin-41(tn1541tn1638)*, *lin-41(tn1541tn1641)*, *lin-41(tn1541tn1643)*, *lin-41(tn1541tn1645)*, *lin-41(tn1541tn1661)*, *lin-41(tn1541tn1663)*, *lin-41(tn1541tn1665)*, *lin-41(tn1541tn1668)*, *lin-41(tn1541tn1684)*, *lin-41(tn1541tn1775)*, *lin-41(tn1767)*, *fog-3(q470)*, and *lin-11(n566)*. LGIII – *mpk-1(ga111*ts*)*, *emb-30(tn377*ts*)*, *cdk-1(ne2257*ts*)*, *orc-1(tn1732[mng::3xflag::orc-1])* and *cul-2(or209*ts). LGIV – *pgl-1(sam37[pgl-1R765S::mTagRFPT::3xflag)* (kindly provided by Dustin Updike), *cks-1(ne549*ts*)*, and *oma-1(zu405te33)*. LGV – *spn-4(tn1699[spn-4::gfp::3xflag])*, *oma-2(te51)*, *oma-2(cp145[mng::3xflag::oma-2])*, *oma-2(tn1760[mng::3xflag::degA::oma-2])*, *oma-2(tn1764[mng::3xflag::degA::degB::oma-2])*, *lon-3(e2175)*, *sel-10(ar41)*, *sel-10(ok1632)*, *sel-10(n1077)*, *him-5(e1490)*, and *fog-2(oz40)*. LGX – *meg-1(tn1724[gfp::3xflag::meg-1])*. The following rearrangements were used: *hT2[bli-4(e937) let-?(q782) qIs48]* (I; III) and *nT1[qIs51]* (IV; V). The following transgene insertions were used: *axIs1498[pie-1p::gfp::gld-1::gld-1 3'UTR, unc-119(+)]*(Merritt *et al.* 2008), *itIs37[pie-1p::mCherry::H2B::pie-1 3'UTR, unc-119(+)]* (McNally

189 *et al*. 2006)*, ozIs5[gld-1::gfp]* I (kindly provided by Tim Schedl), *ozIs2[gld-1::gfp]* II (Schumacher
190 *et al*. 2005), and *pwIs116[rme-2p::rme-2::gfp::rme-2 3'UTR, unc-119(+)]* (Balklava *et al*. 2007).

191

192 ***Genome editing***

193 Plasmids capable of expressing guide RNAs (gRNAs) that target the *lin-41* gene were generated
194 as described by Arribere *et al*. (2014) from the vector pRB1017 and sequence-specific
195 oligonucleotides. We estimated the efficiency with which each *lin-41* gRNA was able to target
196 the *lin-41(tn1541)* locus by: (1) co-injecting a mixture of the gRNA plasmid (25 ng/μl), the
197 pDD162 plasmid (Dickinson *et al*. 2013), which supplies the Cas9 enzyme (50 ng/μl), and a co-
198 injection marker (*myo-2p::Tdtomato*, 4 ng/μl) into *lin-41(tn1541)* hermaphrodites, (2) culturing
199 individual F1 progeny that expressed the co-injection marker (typically ≤10 F1s from each
200 injected parent), and (3) determining the number of F1s that segregated F2 progeny with a Dpy
201 *lin-41* loss-of-function (lf) phenotype. File S1 reports the sequences and estimated efficiencies
202 of the gRNAs we used to generate the *lin-41* deletions and point mutations described in this
203 work; most were relatively effective at targeting *lin-41*.

204 During the efficiency experiments for *lin-41* gRNAs #10 and #11, we identified *lin-*
205 *41(tn1541tn1562)* and *lin-41(tn1541tn1571)*, respectively, as GFP::LIN-41-positive *lin-41(lf)*
206 mutants that appeared to have relatively large deletions by PCR. All of the other deletions were
207 generated in a targeted manner by co-injecting two or more *lin-41* gRNA plasmids (25 ng/μl
208 each), a single-stranded oligonucleotide (ssODN) repair template (500 nM), the pDD162
209 plasmid (50 ng/μl), and a co-injection marker (*myo-2p::Tdtomato*, 4 ng/μl) into *lin-41(tn1541)*

hermaphrodites. We used gRNAs on each side of the desired deletion that, in most cases, would not produce substrates for Cas9 digestion after the deletion event. Otherwise, silent mutations were included in the repair template to prevent re-cutting. To identify *lin-41(tn1541)* deletion mutants, we individually placed F1 worms expressing the co-injection marker on plates, allowed them to lay eggs, and then used PCR to screen pools of up to 6 F1 worms. Pools that appeared to be strongly positive for the desired deletion band were rescreened by PCR to identify F1 animals that had segregated candidate deletion mutants among their F2 progeny. Mutants were either allowed to become homozygous or were balanced using *hT2[bli-4(e937) let-?(q782) qIs48]* (I; III). Essentially the same method was used to generate amino acid substitutions in *lin-41*. However, in those experiments we used only one gRNA and repair events were identified using silent mutations that created restriction enzyme recognition sites in each repair template. Screening therefore consisted of PCR followed by a restriction enzyme digestion, and we only pooled 2 F1s in the initial round of screening so that the repair events would be easy to detect. All edited loci were validated by sequencing, and we were able to obtain multiple independent alleles for most targeted deletions and amino acid substitutions. Where possible, two alleles identical to the repair template (but derived from independently injected parents) were saved and assigned allele names. Other, typically imperfect, gene edits were also kept and given allele names if they were informative or potentially useful. Additional information about all of these alleles, as well as detailed genome editing information, including gRNA, repair template, and PCR primer sequences, is provided in File S1.

oma-2 (tn1760) and *oma-2(tn1764)* were created using the method described by Dickinson *et al*. (2015) to create *oma-2(cp145)*. Indeed, we were careful to replicate *oma-*

232 *2(cp145)* as closely as possible; we used the same gRNA plasmid (pDD223) and designed our
233 repair templates to closely mimic pDD271, the repair template used to create *oma-2(cp145)*.
234 However, instead of using PCR to generate the 3' homology arms of the repair templates, which
235 contain sequences derived from both *oma-2* and *lin-41*, we synthesized these sequences as
236 gBlocks (Integrated DNA Technologies, Skokie, IL). We minimized the size and complexity of
237 each gBlock by removing introns from the *lin-41*-encoding sequences. *oma-2(tn1760)* and *oma-*
238 *2(tn1764)* were perfect matches to the desired repairs (repair templates pCS557 and pCS561,
239 respectively). Gene edited alleles were out-crossed to the wild type before analyzing fertility
240 and embryonic lethality. Specific genome editing details are provided in File S1.

241

242 ***Microscopy***

243 Movies of GFP::LIN-41, mNG::Deg-A::Deg-B::OMA-2, PGL-1::RFP, and mCHERRY::H2B during the
244 OET were obtained using a Marianas 200 Microscopy Workstation (Intelligent Imaging
245 Innovations) built on an AxioObserver Z.1 stand (Carl Zeiss, Thornwood, NY) and driven by
246 SlideBook 6.0 software (Intelligent Imaging Innovations, Denver, CO). The imaging was
247 performed using a 40x oil Carl Zeiss Plan-Apochromat objective lens (numerical aperture of 1.4)
248 and an Evolve electron-multiplying charge-coupled device camera (Photometrics, Tucson, AZ).
249 The quantification of GFP::LIN-41 in proximal oocytes and embryos relative to distal oocytes
250 was performed using ImageJ software. All of the other images were acquired on a Carl Zeiss
251 motorized Axioplan 2 microscope with a 63X Plan-Apochromat (numerical aperture 1.4)
252 objective lens using a AxioCam MRm camera and AxioVision software (Carl Zeiss). Image

quantifications were also performed using AxioVision, version 4.8.2.0. The average intensity of SPN-4::GFP fluorescence was measured in a ~12 μM diameter circle in the anterior cytoplasm of 1-cell and 2-cell embryos in order to avoid the bright puncta of SPN-4::GFP in the posterior; these are likely P granules, as SPN-4 is known to associate with these non-membrane-bound organelles in embryos (Ogura *et al*. 2003). The amount of diffusely cytoplasmic SPN-4::GFP appeared to be similar throughout the embryo during these early stages of embryogenesis and in each of the strains we analyzed. Likewise, the average intensity of GFP::MEX-3 and mNG::OMA-2 fluorescence was measured in a ~10 μM diameter circle in the oocyte cytoplasm. Fluorescence was measured in the oocytes that expressed detectable levels of each fusion protein under our imaging conditions (100 ms and 120 ms for GFP::MEX-3 and mNG::OMA-2, respectively) and were large enough to fit a ~10 μM diameter circle in the oocyte cytoplasm. GFP::MEX-3 was detected in 4 or 5 proximal oocytes in all strains, consistent with previous observations (Tsukamoto *et al*. 2017). mNG::OMA-2 was detected in 5 or 6 proximal oocytes in the *sel-10(ar41)* mutants and in 7 or more proximal oocytes in the control strain.

RNA interference

Gene-specific RNA interference (RNAi) was performed by feeding *C. elegans* with double-stranded RNA (dsRNA)-expressing *E. coli* (Timmons and Fire 1998) at 22^{o} using the RNAi culture media described by Govindan *et al*. (2006). RNAi clones were obtained from Source BioScience (Nottingham, UK), and the identity of each RNAi clone verified by DNA sequencing. The RNAi clone used for *cul-2(RNAi)* targets the *cul-2* 3'UTR, which may make it less effective at triggering

an RNAi response. Exposure to dsRNA-expressing *E. coli* was initiated during the fourth larval stage and GFP::LIN-41 was examined after 1 and 2 days. *cdk-1(RNAi)*, *skr-1(RNAi)* and *sel-10(RNAi)* at least partially prevented the elimination of GFP::LIN-41 after 1 day, with stronger and more penetrant phenotypic effects on Day 2, while *cul-1(RNAi)* only prevented the elimination of GFP::LIN-41 after 2 days of RNAi treatment. All images of RNAi-treated animals were collected on Day 2.

Western blots

Proteins were separated using NuPage 4–12% Bis-Tris gels or 3-8% Tris-Acetate gels (Invitrogen, Carlsbad, CA) and visualized after western blotting. Blots were blocked with 5% nonfat dried milk. Primary antibodies used to detect proteins were affinity-purified rabbit anti-LIN-41 R214 (1:20,000 dilution) (Spike *et al*. 2014a), guinea pig anti-LIN-41 GP49E (1:4,000 dilution) (Spike *et al*. 2014a), and rabbit anti-GLD-1 (1:3,000 dilution; kindly provided by Sarah Crittenden and Judith Kimble) (Jan *et al*. 1999). Secondary antibodies used for western blots were peroxidase-conjugated donkey anti-guinea pig (1:40,000 dilution) (Jackson ImmunoResearch, West Grove, PA) and anti-rabbit (1:5,000 dilution) (Thermo Scientific, Waltham, MA) antibodies. Detection was performed using SuperSignal West Femto Maximum Sensitivity Substrate (Thermo Scientific).

294 ***Antibody staining***

295 Dissected gonads stained with either the rabbit anti-phospho-histone H3 (Ser10) antibody
296 (1:400 dilution; Millipore, Burlington, MA) or the rabbit anti-RME-2 antibody (1:50 dilution,
297 kindly provided by Barth Grant) (Grant and Hirsh 1999) were fixed in 3% paraformaldehyde for
298 1 hour, as described (Rose *et al.* 1997). Dissected gonads stained with the rabbit anti-GLD-1
299 primary antibody (1:150 dilution; Jan *et al*. 1999) were fixed in 1% paraformaldehyde for 10
300 minutes. Primary antibodies were detected using either Cy3-conjugated goat anti-rabbit or
301 Alexa 488-conjugated donkey anti-rabbit secondary antibodies (1:500 dilutions; Jackson
302 ImmunoResearch).

303

304 ***Data availability***

305 All strains and newly-created alleles (see Table S1 and File S1) are available upon request. The
306 sequences of gRNAs, repair templates, PCR primers, *lin-41* alleles, and *oma-2* alleles are
307 presented in File S1. Plasmids producing gRNAs and those containing repair templates for
308 genome editing are available upon request. All Sanger sequencing files are available upon
309 request. Supplemental materials are available at Figshare: https://doi.org/.

310

RESULTS

GFP::LIN-41 is eliminated during the first meiotic division

Germline-expressed LIN-41 is restricted to oogenesis and required to prevent premature M-phase entry and to promote growth of developing oocytes (Spike *et al*. 2014a). In the oogenic germlines of adult hermaphrodites, LIN-41 is expressed from mid-pachytene through subsequent stages of oocyte development, with a notable reduction in LIN-41 levels as oocytes initiate meiotic maturation at the end of oogenesis. Essentially the same pattern is seen in the oocytes of *lin-41(tn1541[gfp::tev::s-tag::lin-41])* adult hermaphrodites; these animals carry a *gfp*-tagged allele of *lin-41* and express only GFP-tagged LIN-41 (GFP::LIN-41), yet have essentially wild-type oocyte development and fertility (Figure 1, A and B; Spike *et al*. 2014a). GFP::LIN-41 is always visible in the oocyte immediately adjacent to the spermatheca (–1 oocyte), but is not detectable in most embryos, suggesting that GFP::LIN-41 is eliminated soon after meiotic maturation and ovulation (Figure 1, A and B; Spike *et al*. 2014a). To more precisely determine the stage at which GFP::LIN-41 is eliminated during the OET, we used time-lapse imaging to examine GFP::LIN-41 as oocytes proceed through meiotic maturation, are ovulated into and fertilized in the spermatheca, and complete their meiotic divisions (Movie S1 and Figure 1, C–H). These images show that GFP::LIN-41 levels drop dramatically after meiotic maturation and ovulation (Figure 1, D and H) and that GFP::LIN-41 is essentially undetectable well before the end of the first meiotic division (Figure 1, F and G). We were able to image several oocytes as they moved into the –1 oocyte position from a slightly earlier developmental stage (–2 or –3 oocyte start position) and completed meiosis. Quantification of GFP::LIN-41

levels in these oocytes revealed that GFP::LIN-41 levels also decline during the late stages of oogenesis, albeit in a somewhat less-dramatic fashion than after meiotic maturation (Figure 1H). During meiotic maturation, the oocyte undergoes a cortical cytoskeletal rearrangement prior to ovulation (McCarter *et al*. 1999). During cortical rearrangement, we observed that GFP::LIN-41 began to localize to punctate structures in the oocyte cytoplasm coincident with the onset of its dramatic disappearance (Movie S1). The nature of these punctate structures is unclear; however, they do not appear to be P granules as most of them do not exhibit colocalization with PGL-1::RFP (Figure S1, A–C).

Deg-A and Deg-B are required to eliminate GFP::LIN-41 from embryos

To identify the amino acid sequences of LIN-41 required for its elimination from early embryos, we generated a series of deletions in the coding region of the GFP::LIN-41-expressing *lin-41(tn1541)* gene using CRISPR-Cas9-based genome editing approaches (see Materials and Methods and File S1 for details). Collectively, these deletions are predicted to remove 95% of the LIN-41 protein and disrupt all known structural domains of LIN-41 (Figure 2, A and B, and File S1). For each mutant, GFP::LIN-41[Δ] expression was examined to determine whether the deleted portion of LIN-41 is necessary for the elimination of GFP::LIN-41 from embryos (Figure 2, D–F, Figure S2, and Figure S3). Null mutations in *lin-41* are sterile, with small, abnormal oocytes, and some hypomorphic alleles of *lin-41* affect the production of high-quality oocytes (Slack *et al*. 2000; Spike *et al*. 2014a). Thus, GFP::LIN-41[Δ] was often examined in both heterozygotes (*lin-41(tn1541Δ)/unc-13(e1091) lin-11(n566)* genotypes) and homozygotes (*lin-*

353 *41(tn1541Δ)* genotypes), particularly when the *lin-41(tn1541Δ)* homozygotes produced
354 obviously small or abnormal oocytes or produced a significant number of dead embryos (Figure
355 S2, Figure S3, and Table 1). This approach enabled us to determine that two non-overlapping
356 regions in the N-terminal third of LIN-41 are required for the elimination of LIN-41 from
357 embryos (Figure 2B). We will refer to these regions as the LIN-41 degradation domains Deg-A
358 and Deg-B.

359 The LIN-41 Deg-A domain is defined by the *lin-41(tn1541tn1638)* deletion allele. This
360 deletion is predicted to affect GFP::LIN-41 by removing 73 amino acids on the N-terminal side
361 of the LIN-41 RING domain (Figure 2C and File S1). *lin-41(tn1541tn1638)* is immediately
362 adjacent to, but does not overlap, the *lin-41(tn1541tn1630)* deletion, which is predicted to
363 affect GFP::LIN-41 by removing the LIN-41 RING finger domain (see File S1 for deleted residues).
364 Consistent with previous amino acid substitution and transgenic rescue data (Tocchini *et al*.
365 2014), the RING domain is not required for the elimination of GFP::LIN-41 from embryos (Figure
366 2E and Figure S2). The LIN-41 Deg-B domain is defined by two contiguous, but non-overlapping,
367 deletions on the C-terminal side of the LIN-41 RING domain. The *lin-41(tn1541tn1635)* deletion
368 is predicted to affect GFP::LIN-41 by removing 44 amino acids on the C-terminal side of the LIN-
369 41 RING domain (Deg-B1) (Figure 2C and File S1). Compared to the Deg-A deletion mutant (*lin-*
370 *41(tn1541tn1638)*), the Deg-B1 deletion mutant (*lin-41(tn1541tn1635)*) has a relatively low but
371 detectable level of GFP::LIN-41[Δ] in early embryos (compare Figure S2, K and M). However, the
372 *lin-41(tn1541tn1622)* deletion, which defines Deg-B2, and the remaining 151 amino acids of
373 Deg-B (Figure 2C and File S1), has a robust defect in the elimination of GFP::LIN-41[Δ] from
374 early embryos that is apparent in both heterozygous and homozygous deletion mutants (Figure

S2, E and G). Finally, deletions predicted to affect GFP::LIN-41 by removing amino acids and structural domains C-terminal to Deg-B were able to eliminate GFP::LIN-41[Δ] from early embryos (Figure 2A and Figure S3). Interestingly, we found that C-terminal domains could only be removed individually or in small groups, as GFP::LIN-41[Δ] was not detectable when a majority of the C-terminus was removed (*lin-41(tn1541tn1628)* deletion; Figure 2A and Figure S3, M–P).

LIN-41[T83] is required to eliminate LIN-41 from embryos

The results described above indicate that the elimination of GFP::LIN-41 does not depend on any of the previously described structural domains of LIN-41, but instead requires two new regulatory domains. Analysis of the amino acid sequences of Deg-A and Deg-B shows that each regulatory domain contains many possible phosphorylation sites (Figure 2C). Previously published results indicate that the elimination of GFP::LIN-41 from embryos also requires CDK-1 (Spike *et al.* 2014a), a highly conserved proline-directed serine/threonine kinase essential for M-phase entry during oocyte meiotic maturation in *C. elegans* (Boxem *et al*. 1999). Thus, we hypothesized that LIN-41 might be a direct target of CDK-1 activity, and that phosphorylation of either Deg-A or Deg-B by CDK-1 could be sufficient to trigger the elimination of GFP::LIN-41 from embryos. 18 minimal CDK-1 consensus sequences ([S/T]P) are present in Deg-A and Deg-B (Figure 2C), but only a single site, found in Deg-B1, conforms to an expanded CDK1 consensus sequence ([S/T]PX[K/R]) (Ubersax *et al.* 2003). However, changing the potentially

phosphorylated residue at this site to an alanine (S176A; e.g.: *lin-41(tn1541tn1641)*) had no effect on the elimination of GFP::LIN-41 from embryos (Figure 2C and Figure S4A).

We therefore shifted our focus to Deg-A, which is relatively small and contains only three potential CDK-1 target sites, but strongly prevents the elimination of GFP::LIN-41 from embryos (Figure S2M). Each site in Deg-A was tested individually to see if it is required for the elimination of GFP::LIN-41 from embryos. Although the mutations S57A and S90A (e.g.: *lin-41(tn1541tn1663)* and *lin-41(tn1541tn1661)*, respectively) had no discernable effect (Figure S4, C and E), the T83A mutation (e.g.: *lin-41(tn1541tn1645)*) strongly prevented the elimination of GFP::LIN-41 from embryos, similar to the Deg-A deletion mutant (Figure 2G, Figure S2M, and Figure S4G). Time-lapse imaging of oocyte meiotic maturation, ovulation, and fertilization documents that the T83A mutation strongly abrogates the elimination of GFP::LIN-41 (Movie S2). During cortical rearrangement, GFP::LIN-41[T83A] localized partially to dynamic punctate structures like GFP::LIN-41 (compare Movie S1 and Movie S2); however unlike the wild-type protein, puncta of GFP::LIN-41[T83A] were also observed during the meiotic divisions. Furthermore, GFP::LIN-41[T83A] persisted through multiple embryonic cleavage divisions and became at least partially associated with P granules by the 2-cell stage (Movie S2 and Figure S1, D–I). These results are consistent with the possibility that phosphorylation of LIN-41 by a proline-directed S/T kinase, such as CDK-1, promotes the rapid elimination of GFP::LIN-41 upon the onset of meiotic maturation. As a further assessment, we replaced T83 with a glutamic acid residue (T83E) (e.g.: *lin-41(tn1541tn1684)*), which is negatively charged and might function as a phosphomimetic. However, T83E did not result in the premature elimination of GFP::LIN-41, as when CDK-1 is prematurely activated (Spike *et al*. 2014a). Instead, T83E prevented the

417 elimination of GFP::LIN-41 from embryos, similar to T83A (Figure S4, G and I). Thus, we
418 conclude that either T83E does not effectively mimic phosphorylation at this particular site or
419 T83 might not be phosphorylated. In fact, phosphorylation sites that function to recruit adapter
420 proteins are often not recognized by binding partners after phosphomimetic substitution
421 (Dephoure *et al*. 2013), and this is a possible explanation for the function of T83 and the Deg
422 domains of LIN-41, as we will describe.

423 A requirement for the extreme N-terminus of LIN-41 (amino acids 1–39) with respect to
424 the elimination of GFP::LIN-41 was not examined in the *lin-41(tn1541)* deletion analysis.
425 Genetic analysis suggests that this region of LIN-41 is important for down-regulating *lin-41*
426 function specifically in the male tail (Del Rio-Albrechtsen *et al*. 2006). Gain-of-function (gf)
427 alleles that affect this part of LIN-41 have a defect in male tail tip retraction, while
428 hermaphrodites appear overtly wild-type. *lin-41(tn1541)* males also have a male tail tip
429 retraction defect (Figure S5, A and B), suggesting that the GFP tag on the N-terminus of LIN-41
430 disrupts this male-specific function. Furthermore, the amino acid change found in the *lin-*
431 *41(bx37*gf*)* allele (G35R) does not affect the elimination of GFP::LIN-41 from early embryos (*lin-*
432 *41(tn1541tn1665);* Figure S5, C and E). For these reasons, we suspect that the extreme N-
433 terminus of LIN-41 is unlikely to be involved in the elimination of GFP::LIN-41 from early
434 embryos. One possibility, however, might be that the N-terminal GFP tag on GFP::LIN-41
435 compromises a function that is required redundantly with Deg-A or Deg-B. To explore this
436 possibility, we generated worms expressing LIN-41[T83A] (*lin-41(tn1767)*) and asked whether
437 the untagged protein also persists in embryos. Using western blots, we found that LIN-41 was
438 undetectable in a lysate made from wild-type embryos, but that LIN-41[T83A] was clearly

present in a lysate prepared from *lin-41(tn1767)* mutant embryos (Figure S6C). Thus, the T83A mutation abrogates the elimination of both LIN-41 and GFP::LIN-41 from embryos.

Functional requirements for individual LIN-41 domains

LIN-41 is a large protein with two well-defined domains that are proposed to have strikingly different activities. The first of these is actually a multi-domain grouping called a TRIpartite Motif (TRIM) that contains RING, B-box, and coiled-coil (CC) domains; many TRIM proteins are thought to function as RING finger E3 ubiquitin ligases (Ikeda and Inoue 2012). The second functional domain is an RNA-binding domain composed of 6 NHL (NCL-1, HT2A and LIN-41) repeats at the C-terminus of LIN-41 (Slack and Ruvkun 1998; Loedige *et al*. 2015; Kumari *et al*. 2018). Forward and reverse genetic analyses strongly indicate that the NHL domain is important for both the germline and somatic functions of *C. elegan*s LIN-41 (Slack *et al*. 2000; Spike *et al*. 2014a; Tocchini *et al*. 2014), consistent with the identification of LIN-41 as a translational repressor in both tissue types (Spike *et al*. 2014b; Aeschimann *et al*. 2017; Tsukamoto *et al*. 2017). By contrast, a deletion of the entire LIN-41 RING domain (Figure 2A), which confers *in vitro* E3 ligase catalytic activity to mouse LIN41 and other TRIM proteins (Rybak *et al*. 2009; Esposito *et al*. 2017), results in appreciable fertility (brood size of 210 ± 87; Table 1) and thus is non-essential for *C. elegans* oogenesis. As described below, the phenotypes seen in *lin-41(tn1541)* deletion mutants are consistent with prior observations and provide additional insights into the functions of LIN-41 protein domains.

TRIM (Ring, B-box, CC) domain: Deletion of the RING finger in the context of GFP::LIN-41 (GFP::LIN-41[ΔRING]) results in only mild defects. Most *lin-41(tn1541tn1630)* animals are fertile and have a large number of progeny; no strong defects in oogenesis, embryonic development or body shape are evident (Table 1 and Figure S2, I and J). We did note, however, that *lin-41(tn1541tn1630)* animals appear to be slightly sick and that they produce ~33% fewer progeny than *lin-41(tn1541)* hermaphrodites (Table 1). Interestingly, deletion of the other two TRIM sub-domains (GFP::LIN-41[ΔBbox-CC]) causes a much stronger reduction in LIN-41 function. Most (84%) *lin-41(tn1541tn1562)* hermaphrodites are fertile, but produce very few progeny (6 ± 4) and have obvious defects in oogenesis as well as a Dumpy (Dpy) body shape (Table 1; Figure S3, A and B). Thus, *lin-41(tn1541tn1562)* is clearly a hypomorphic allele of *lin-41* that affects both its germline and somatic functions.

We note that *lin-41(tn1541tn1562)* might remove additional residues beyond the Bbox-CC region because, unlike the other *lin-41(tn1541Δ)* mutants we created, *lin-41(tn1541tn1562)* is not a precise exon-exon fusion and requires a new in-frame splicing event to make a full-length protein (Figure 2A and File S1). However, the deletion in this mutant was accompanied by the insertion of a small sequence that includes two potential 5' splice site consensus sequences; both are in-frame with the downstream exon. Furthermore, the relative size of GFP::LIN-41[ΔBbox-BBC] on SDS-PAGE western blots is consistent with what we expect to see for the protein made by this particular deletion mutant (File S1 and Figure S6B). This is also true for the other GFP::LIN-41[Δ] proteins we detected on western blots using anti-LIN-41 antibodies (Figure S6, A and B).

480 ***IG/filamin domain:*** IG/filamin (IG) domains are only found in a subset of TRIM-NHL proteins;
481 structural analysis of this part of *C. elegans* LIN-41 suggests that it forms a classic IG-like domain
482 fold (Tocchini *et al.* 2014). The IG domain has been proposed to function, along with the coiled-
483 coil domain, as a binding platform for proteins that repress the translation of NHL-bound target
484 mRNAs (Loedige *et al*. 2013). *lin-41(ma104)* is a hypomorphic allele that likely disrupts the
485 structure and function of the LIN-41 IG domain (Tocchini *et al.* 2014). As previously reported
486 (Spike *et al*. 2014b), outcrossed *lin-41(ma104)* mutant hermaphrodites have mild oocyte
487 defects and a reduced, but still substantial, brood size of 181 progeny (n=12). Deletion of the IG
488 domain in the context of GFP::LIN-41 (GFP::LIN-41[ΔIG]) results in stronger defects. Most *lin-*
489 *41(tn1541tn1571)* hermaphrodites are fertile, with a very low brood size (11 progeny) and
490 obvious defects in oogenesis (Table 1 and Figure S3, C and D). Both alleles also result in worms
491 with an obviously Dpy body shape. Thus, despite the difference in brood size, the alleles that
492 affect the IG domain are hypomorphic and reduce both the germline and somatic functions of
493 *lin-41*. Indeed, it is potentially misleading to conclude that the relative severities of *lin-*
494 *41(ma104)* and *lin-41(tn1541tn1571)* are meaningful, as LIN-41 function may be slightly
495 compromised in the *lin-41(tn1541)* mutant despite its wild-type brood size (316 ± 39; Table 1;
496 Spike *et al*. 2014a). For example, the introduction of the LIN-41[D1125N] amino acid change
497 that results in a temperature-sensitive (ts) phenotype in an otherwise wild-type LIN-41 protein
498 (e.g.: *lin-41(tn1487(*ts*);* 100% fertile at 15^{o}C (n=224), average brood size of 104 (n=64); Spike *et*
499 *al.* 2014a) results in a stronger, but still hypomorphic, phenotype in a GFP::LIN-41 mutant
500 background (e.g.: *lin-41(tn1541tn1548)*; 71% fertile at 15^{o}C (n=21), average brood size of 3
501 (n=15)).

The NHL domain: Deletion of the C-terminal NHL domain in the context of GFP::LIN-41 (GFP::LIN-41[ΔNHL]) results in a strong loss-of-function *lin-41* phenotype. Whereas *lin-41(tn1541)* hermaphrodites are fertile, with normal oocyte development and overall appearance, nearly all (98.5%) *lin-41(tn1541tn1618)* hermaphrodites are sterile and have a Dpy body shape (Table 1). Oogenesis is extremely abnormal in most animals (Figure S3, G and H), although *lin-41(tn1541tn1618)* hermaphrodites appear capable of producing embryos on occasion (Table 1 and Figure S3, I and J). The fact that deletion of the LIN-41 NHL domain does not result in 100% sterility is surprising because the *lin-41(n2914)* null mutation has never been observed to produce progeny. Thus, LIN-41 can exhibit some, albeit very low, biological function in the absence of the NHL domain. We suggest, that this low-level function may be mediated through components of the LIN-41 RNP (Spike *et al.* 2014b; Tsukamoto *et al*. 2017). We confirmed that CDK-1 exhibits premature activation in post-dauer *lin-41(tn1541tn1618)* mutants, as it does in *lin-41(n2914)* null mutants, by staining adult hermaphrodite germlines with an antibody specific to histone H3 phosphorylated on Serine 10 (pH3(S10)). This antibody stains the nucleoplasm and condensed chromosomes of wild-type diakinesis-stage oocytes as they prepare enter M-phase near the spermatheca (Hsu *et al*. 2000). Both M-phase and anti-pH3(S10) staining occur prematurely in strong loss-of-function *lin-41* mutants and are *cdk-1*-dependent (Spike *et al*. 2014a). As expected for a strong loss-of-function mutant, and consistent with the idea that premature M-phase entry and CDK-1 activation occur prematurely, we detected pH3(S10)-positive condensed chromosomes in or near the loop region of the gonad, and just after the end of pachytene, in most *lin-41(tn1541tn1618)* oogenic germlines (n=6/9). Interestingly, GFP::LIN-41[ΔNHL] forms abnormal aggregates in the oocytes

of *lin-41(tn1541tn1618)* homozygotes; these aggregates are not seen in heterozygotes (Figure S3, G, I, and K). The reason for this aberrant pattern of localization is unknown, but GFP::LIN-41[ΔNHL] aggregation is also seen in post-dauer *lin-41(tn1541tn1618)*; *cdk-1(RNAi)* animals (n=32), and therefore does not depend on the dysregulation of *cdk-1* function that occurs during oogenesis in strong loss-of-function *lin-41* mutants (Spike *et al*. 2014a). These aggregates may reflect abnormal biogenesis of LIN-41 RNPs in the absence of the NHL domain.

Meiotic degradation domains are nonessential: We initially hypothesized that the deletion of LIN-41 degradation domains might result in a gain-of-function phenotype that would impact fertility or embryonic viability. However, *lin-41(tn1541tn1643)*, a large deletion that removes Deg-A, the RING finger, and Deg-B in the context of GFP::LIN-41, behaves as a recessive hypomorph that preferentially affects germline function. Homozygous mutants do not have a strong Dpy phenotype, but do have an extremely small brood size and display obvious defects in oogenesis and embryogenesis (Table 1 and Figure S2, O and P). In contrast, heterozygous *lin-41(tn1541tn1643)* mutants appear essentially normal (n=20). This is also true for deletions that subdivide the large N-terminal region of LIN-41, such as *lin-41(tn1541tn1620)* and *lin-41(tn1541tn1622)* (Table 1 and Figure S2, A–H). Indeed, even when homozygous, the relatively small Deg-A deletion (*lin-41(tn1541tn1638)*), which results in abundant GFP::LIN-41[ΔDeg-A] in early embryos, appears to have minimal consequences for GFP::LIN-41 function at 20^{o} (Table 1 and Figure S2, M and N). Likewise, animals expressing LIN-41[T83] and GFP::LIN-41[T83] appear essentially wild-type; the latter have only a slightly reduced brood size relative to GFP::LIN-41-expressing controls (Table 1 and Figure S4, G and H). Consequently, we decided to look carefully at the ovulation rates of the minimally affected LIN-41 Deg-A deletion (*lin-41(tn1541tn1638)*)

546 and T83A point mutants (*lin-41(tn1541tn1645)* and *lin-41(tn1767)*). Oocyte meiotic maturation
547 is a rate-limiting step for hermaphrodite fertility and the ovulation rate approximates the rate
548 of oocyte meiotic maturation (McCarter *et al.* 1999; Miller *et al*. 2001, Govindan *et al*. 2006).
549 Importantly, several aspects of nuclear and cytoplasmic oocyte maturation occur prematurely
550 in *lin-41(lf)* mutations (Spike *et al*. 2014a,b; Tsukamoto *et al*. 2017). Deg-A domain mutants
551 exhibit mean ovulation rates that are significantly reduced relative to genotype-matched
552 controls (Figure 2H). Interestingly, the mean ovulation rate of the *lin-41(tn1541)* control strain
553 was elevated relative to wild-type animals (Figure 2H, 3.4 vs 2.9 ovulations/gonad arm/hr).
554 Together, these observations suggest that (1) *lin-41(tn1541)* might be a weak hypomorph that
555 causes a slight increase in the oocyte maturation rate and (2) Deg-A domain mutants cause the
556 opposite phenotype, a reduced oocyte maturation rate. These changes in the rate of oocyte
557 maturation are relatively modest, however, and our phenotypic analyses generally suggest that
558 the elimination of LIN-41 from early embryos is not a critical control point for regulating LIN-41
559 function or activity levels *in vivo*.

560

561 ***LIN-41[Deg] domains are sufficient for degradation***

562 OMA-1 and OMA-2 (OMA-1/2) are functionally redundant cytoplasmic RNA binding proteins
563 expressed in oocytes and early embryos (Detwiler *et al.* 2001) that co-purify with LIN-41 RNP
564 complexes (Spike *et al*. 2014b, Tsukamoto *et al*. 2017). OMA-1/2 levels remain high in 1-cell
565 embryos until the first mitotic division, when they are rapidly degraded (Lin 2003; Nishi and Lin
566 2005; Shirayama *et al*. 2006; Stitzel *et al*. 2006). The expression and subsequent elimination of

OMA-2 can be easily visualized in *oma-2(cp145)* mutants (Dickinson *et al.* 2015; Figure 3A and Figure S7, A and B), which express an mNeonGreen-tagged form of OMA-2 that is largely functional *in vivo* (Table 2, compare *oma-1(zu405te33); oma-2(cp145)* to *oma-1(zu405te33); oma-2(te51)* and *oma-1(zu405te33)*). Based on these attributes, we decided to test whether the LIN-41 Deg domains are sufficient to induce the premature degradation of mNG::OMA-2 during meiosis. Molecularly, we chose to place LIN-41 DEG domains between mNeonGreen and OMA-2 (Figure 3, A–C), as this is similar to their locations in GFP::LIN-41 (Figure 2, A and B) and no structural (e.g., X-ray crystallographic) data are available to aid the experimental design. Using the same method that Dickinson *et al.* (2015) used to make *oma-2(cp145)*, we created two new *oma-2* alleles that also contain *lin-41*-encoded Deg domains and examined the pattern of mNG::DEG::OMA-2 accumulation prior to the first mitotic division (Figure 3 and Figure S7).

We began by testing LIN-41 Deg-A, which contains the possible CDK-1 target site (T83) required for the elimination of LIN-41. *oma-2(tn1760)* mutants express mNG::Deg-A::OMA-2 in oocytes and 1-cell embryos. Similar to mNG::OMA-2, this protein is present in 1-cell embryos just prior to the first mitotic division but eliminated from older embryos (Figure 3, D and E, and Figure S7, A, B, E, and F). Indeed, the only obvious difference was the amount of mNG in older 1-cell pronuclear stage embryos, which was significantly reduced in *oma-2(tn1760)* embryos compared to *oma-2(cp145)* controls (compare Figure 3, D and E, and Figure S8A). This reduction might be caused by Deg-A-mediated destabilization of the mNG::OMA-2 fusion protein (see below), but is not equivalent to the rapid elimination of GFP::LIN-41 that occurs in meiosis I (Movie S1 and Figure 1). Because Deg-A on its own was not sufficient to trigger the rapid elimination of mNG::OMA-2 in 1-cell embryos, we tested LIN-41 Deg-A and Deg-B together.

589 *oma-2(tn1764)* mutants express mNG::Deg-A, Deg-B::OMA-2 in oocytes, but in 1-cell embryos
590 the amount of mNG is substantially reduced or absent (Figure 3F and Figure S7, G and I). To
591 more precisely determine the stage at which mNG::DEG-A, Deg-B::OMA-2 is eliminated, we
592 used time-lapse imaging (Movie S3 and Figure 3, L–O). Levels of this fusion protein drop
593 somewhat during the first meiotic division (Figure 3, M and N) and become essentially
594 undetectable before the end of the second meiotic division (Figure 3O). We conclude that Deg-
595 A and Deg-B are sufficient in combination to trigger the rapid degradation of mNG::OMA-2
596 during meiosis, although this event is temporally delayed relative to GFP::LIN-41 (Figure 3P).

597 *oma-1* and *oma-2* share redundant functions during both oocyte and early embryo
598 development (Detwiler *et al*. 2001; Guven-Ozkan *et al*. 2008). Double mutants carrying strong
599 loss-of-function alleles (e.g., *oma-1(zu405te33); oma-2(te51)*) are sterile with a defect in
600 meiotic maturation (Detwiler *et al*. 2001; Table 1). For the most part, the embryonic functions
601 of *oma-1/2* have been studied using conditions that reduce, but do not eliminate, OMA-1/2
602 function in embryos, such as double RNA interference (RNAi) or reduction-of-function alleles
603 that are incompletely sterile (Nishi and Lin 2005; Guven-Ozkan *et al*. 2008). In *oma-*
604 *1(zu405te33)*; *oma-2(tn1764)* double mutants, OMA-2 is expressed during oogenesis but
605 eliminated prematurely from embryos. Consequently, these double mutants are very fertile but
606 produce progeny that die during embryogenesis (Table 2). Thus, as a novel allele that
607 specifically reduces embryonic OMA-2, *oma-2(tn1764)* may be useful for studying the
608 embryonic functions of *oma-1/2*. Our initial observations indicate that young *oma-*
609 *1(zu405te33); oma-2(tn1764)* embryos exhibit cell division defects and ectopic cleavage furrows
610 (Figure S8B); similar defects have been reported after *oma-1/2(RNAi)* depletion (Li *et al*. 2009).

When combined with *oma-1(zu405te33)*, *oma-2(tn1764)* exhibits a stronger embryonic phenotype than either *oma-2(cp145)* or *oma-2(tn1760)*. However, the severity of the *oma-1(te33zu405); oma-2(tn1760)* double mutant phenotype relative to *oma-1(te33zu405); oma-2(cp145)* was somewhat surprising (Table 2; 60 vs. 12% embryonic lethality). One possibility for the stronger embryonic phenotype might be the reduction in mNG::Deg-A::OMA-2 levels observed in *oma-2(tn1760)* pronuclear-stage embryos (Figure 3E and Figure S8A). We examined this more closely by crossing each mNG-tagged *oma-2* allele into an *emb-30(tn377*ts*)* mutant background. *emb-30* encodes a subunit of the Anaphase Promoting Complex (APC), and adult *emb-30(tn377*ts*)* hermaphrodites upshifted to restrictive temperature (25°C) produce 1-cell embryos that arrest in metaphase of the first meiotic division (Furuta *et al*. 2000). Arrest in meiotic metaphase does not prevent or delay the elimination of GFP::LIN-41, which is independent of APC function (Spike *et al*. 2014a). We observed that mNG::OMA-2 is turned over in arrested meiotic embryos, but could typically be seen in 4 embryos in the uterus of *emb-30(tn377ts); oma-2(cp145)* hermaphrodites after a 5–7 hour upshift to 25°C (Figure S8C). In contrast, both of the LIN-41 Deg domain-containing OMA-2 proteins appeared to be less stable under the same conditions. mNG::Deg-A, Deg-B::OMA-2 was seen in 0–1 mNG-positive embryos and appeared to be the least stable (Figure S8E), as expected from our previous analysis (Figure 3 and Figure S7). mNG::Deg-A::OMA-2 was seen in 2 mNG-positive embryos and therefore appeared to be of intermediate stability (Figure S8D). Thus, although Deg-A is not sufficient for rapid elimination, it likely reduces the stability of mNG::Deg-A::OMA-2 in meiotic embryos. The consequent reduction in protein levels could contribute to the stronger *oma-2(tn1760)* embryonic phenotype, although it also seems possible that insertion of LIN-41 Deg-A

633 at the N-terminus of OMA-2 might perturb the nearby TAF-4 binding domain (Figure 3, A–C),
634 which is critical for the function of OMA-2 in embryos (Guven-Ozkan *et al*. 2008).

635

636 ***GFP::LIN-41 is eliminated from embryos by SCF^{SEL-10}***

637 Several different Skp, Cullin, F-box (SCF)-containing E3 ubiquitin ligase complexes promote
638 protein degradation during meiosis and early embryogenesis in *C. elegans* (Peel *et al*. 2012; Du
639 *et al*. 2015; Beard *et al*. 2016). We initially used RNAi to knock down the functions of each of
640 the six cullins identified in the *C. elegans* genome (Kipreos *et al*. 1996; Nayak *et al*. 2002) to
641 determine whether an SCF-type E3 ligase is involved in the elimination of GFP::LIN-41. In
642 general, RNAi was initiated in *lin-41(tn1541)* hermaphrodites at the L4 larval stage and
643 GFP::LIN-41 was examined in adults, two days after the initiation of the RNAi treatment at 22^{o}C.
644 Of the six cullins we tested, only the *cul-1(RNAi)*-treated animals produced multiple young
645 embryos with faint GFP::LIN-41 (n=12), suggesting that CUL-1 may be required to eliminate
646 GFP::LIN-41 from embryos. *rrf-1(pk1417)* mutants are RNAi-defective in certain somatic cells,
647 including the somatic gonad, but are sensitive to RNAi in the germline (Sijen *et al.* 2001; Kumsta
648 and Hansen 2012). Treatment of *rrf-1(pk1417) lin-41(tn1541)* hermaphrodites with *cul-1(RNAi)*
649 also resulted in the failure to eliminate GFP::LIN-41 from early embryos (n=54; Figure 4C).
650 Together, these results suggest that a germline-expressed CUL-1-containing SCF E3 ubiquitin
651 ligase may eliminate GFP::LIN-41 from early embryos. At least three of the *C. elegans* cullins,
652 *cul-1*, *cul*-2 and *cul*-3, are important for normal embryonic development. We observed highly
653 penetrant embryonic lethality after treating *rrf-1(pk1417) lin-41(tn1541)* and *lin-41(tn1541)*

654 animals with *cul-1(RNAi)* and *cul-3(RNAi)*, respectively. However, *cul-2(RNAi)* did not result in
655 any obvious phenotypes. We therefore examined *lin-41(tn1541); cul-2(or209*ts*)* adults
656 upshifted to 25°C as L4s to assess whether *cul-2* is important for the elimination of GFP::LIN-41
657 from embryos. GFP::LIN-41 was eliminated normally from the dead embryos produced by *cul-*
658 *2(or209*ts*)* parents at restrictive temperature (n=71), suggesting that a CUL-2-containing SCF E3
659 ubiquitin ligase is not involved in the elimination of GFP::LIN-41 from embryos.

660 In SCF-type E3 ligases, cullins interact with Skp-1-related proteins. Twenty-one Skp1-
661 related (*skr*) genes have been identified in *C. elegans*, and RNAi experiments suggest the closely
662 related *skr-1* and *skr-2* genes function in the germline and early embryo (Nayak *et al*. 2002;
663 Yamanaka *et al*. 2002; Shirayama *et al.* 2006; Fox *et al*. 2011; Mohammad *et al*. 2018). In
664 addition, both SKR-1 and SKR-2 can interact with CUL-1 (Nayak *et al*. 2002, Yamanaka *et al*.
665 2002). We therefore examined whether *skr-1(RNAi)*, which likely reduces the function of both
666 *skr-1* and *skr-2*, would prevent the elimination of GFP::LIN-41 from early embryos. *lin-*
667 *41(tn1541); skr-1(RNAi)* animals produced embryos with defects in the elimination of GFP::LIN-
668 41 two days after RNAi treatment (n=26; Figure 4B). Treatment of *rrf-1(pk1417) lin-41(tn1541)*
669 animals with *skr-1(RNAi)* also prevented the elimination of GFP::LIN-41 from early embryos
670 (n=14). In addition, the *rrf-1(pk1417) lin-41(tn1541)* mutants treated with *skr-1(RNAi)* for two
671 days at 22°C exhibited defects in germline morphology and embryo production that are
672 consistent with the phenotypes previously described after *skr-1/2(RNAi)* (Nayak *et al*. 2002).

673 At least three F-box-containing substrate recognition subunits, LIN-23, PROM-1, and
674 SEL-10, are thought to function with either SKR-1 or SKR-2 and CUL-1 in the *C. elegans* germline

or early embryos (Peel *et al*. 2012; Du *et al*. 2015; Kisielnicka *et al. 2018*; Mohammad *et al*. 2018). LIN-23, SEL-10 and their vertebrate orthologs (β-TrCP and Fbw7, respectively) regulate the cell cycle and cell cycle-dependent protein degradation (Kipreos *et al*. 2000; Nakayama and Nakayama 2005; Welcker and Clurman 2008; de la Cova and Greenwald 2012). Because the rapid elimination of GFP::LIN-41 appears to be coupled to meiotic maturation, a cell-cycle event, we used RNAi to knock down the activities of *lin-23* and *sel-10* as a first step toward the analysis of candidate F-box proteins. *lin-23(RNAi)* had no effect on the elimination of GFP::LIN-41 from *rrf-1(pk1417) lin-41(tn1541)* embryos (n=52; Figure S9C). Consistent with this observation, mutations designed to prevent the phosphorylation of a possible β-TrCP binding site near the amino-terminus of LIN-41 (amino acids 32–38) also do not prevent the elimination of GFP::LIN-41 from embryos (*lin-41(tn1541tn1668)*; Figure S5, D and E). However, *sel-10(RNAi)* did prevent the elimination of GFP::LIN-41 from *rrf-1(pk1417) lin-41(tn1541)* embryos (n=17). Similarly, the elimination of GFP::LIN-41 from young embryos is prevented by the strong loss-of-function mutations *sel-10(ok1632)* and *sel-10(ar41)* (Figure 4, D, E, G, and I). All of our *sel-10(ar41)* strains also contain *lon-3(e2175)*, a convenient cis-linked marker that encodes a cuticle collagen (Nyström *et al.* 2002; Suzuki *et al*. 2002). GFP::LIN-41 is eliminated normally from *lon-3(e2175)* mutant embryos (Figure 4F). Finally, we observed that *sel-10(n1077)*, which has both gain-of-function and loss-of-function properties (Jäger *et al*. 2004), fails to eliminate GFP::LIN-41 from early embryos (Figure 4J). Genetic and physical interactions indicate that SEL-10 and SKR-1 function together in *C. elegans* (Killian *et al*. 2008; Kisielnicka *et al*. 2018). Because our *skr-1(RNAi)* experiments are likely to also target *skr-2* (Nayak *et al*. 2002), we are unable to parse out the relative roles of SKR-1 and SKR-2 at this time. Collectively, these observations

suggest that a germline-expressed SCF^{SEL-10} E3 ubiquitin ligase containing SKR-1/2, CUL-1 and SEL-10 is likely involved in the elimination of GFP::LIN-41 from early embryos (Figure 5E).

SEL-10 functions through LIN-41 degradation domains

LIN-41 can be detected in *sel-10(ok1632)* mutant but not wild-type embryos by western blot analysis (Figure S6C), indicating that endogenous and GFP-tagged LIN-41 behave similarly. We hypothesized that the Deg domains are likely used to target LIN-41 for degradation by SCF^{SEL-10}. To test this hypothesis, we examined whether the premature elimination of mNG::Deg-A, Deg-B::OMA-2, which is mediated by the LIN-41 Deg domains, is prevented in *sel-10* mutant embryos. Although mNG::Deg-A, Deg-B::OMA-2 is eliminated by the pronuclear stage in otherwise wild-type 1-cell embryos, mNG::Deg-A, Deg-B::OMA-2 levels remain high in *lon-3(e2175) sel-10(ar41)* embryos at the same stage of embryonic development (Figure 3, F, G, J, and K, and Figure S7, G, H, K, and L). As for GFP::LIN-41, this is not caused by the cis-linked marker *lon-3(e2175)* (Figure S7, I and J). These observations suggest that *sel-10(ar41)* should suppress the completely penetrant maternal-effect lethal phenotype exhibited by *oma-1(zu405te33); oma-2(tn1764)* mutants (Table 2). Consistent with this expectation, *oma-1(zu405te33); oma-2(tn1764) lon-3(e2175) sel-10(ar41)* animals produce hatchlings and can be maintained as a homozygous strain (Table 2). However, we note that *sel-10(ar41)* is a relatively weak suppressor of the *oma-1(zu405te33); oma-2(tn1764)* maternal-effect lethal mutant phenotype, since only 10–15% of the embryos produced by *oma-1(zu405te33); oma-2(tn1764) lon-3(e2175) sel-10(ar41)* animals hatch. This observation is consistent with the possibility that

718 mNG::Deg-A, Deg-B::OMA-2 may only be partially functional in the 1-cell embryo. One
719 possibility is that the Deg-A, Deg-B insertion perturbs OMA-2 function. Additionally, *sel-*
720 *10(ar41)* mildly reduces mNG::OMA-2 accumulation in the germline likely through effects on
721 GLD-1 (see below). Although the degradation of OMA-1, and presumably OMA-2, appears to be
722 mediated by several SCF E3 ubiquitin ligases, SEL-10 has not been implicated in this process
723 (Shirayama *et al.* 2006; Du *et al.* 2015). Indeed, mNG::OMA-2 is degraded at the expected time
724 in *oma-2(cp145) lon-3(e2175) sel-10(ar41)* embryos (Figure S7, C and D). Likewise, mNG::Deg-A,
725 Deg-B::OMA-2 levels only remain high until the end of the 1-cell stage in *oma-2(tn1764) lon-*
726 *3(e2175) sel-10(ar41)* embryos, when the degradation of OMA-2 is normally initiated (Figure S7,
727 K and L). We conclude that SEL-10 is not required for the elimination of OMA-2 and likely
728 functions through the LIN-41 Deg domains to promote the proteolytic degradation of LIN-41
729 and mNG::Deg-A, Deg-B::OMA-2 during meiosis.

730

731 ***SEL-10 is required for the CDK-1-dependent elimination of GFP::LIN-41***

732 Substrate recognition subunits such as SEL-10 recognize their targets by binding to short linear
733 sequence motifs called degrons (Lucas and Ciulli 2017). LIN-41 Deg domains were therefore
734 examined for sequences similar to the SEL-10/Fbw7/Cdc4 degron consensus sequence
735 ΦΦ[pT/pS]PXX[pT/pS/E/D], where Φ represents a hydrophobic amino acid. This degron is
736 commonly referred to as a Cdc4 phosphodegron or CPD; it contains two essential residues, a
737 phosphorylated residue that is typically a phosphothreonine, immediately followed by a proline
738 (pTP) (Nash *et al*. 2001). Residues surrounding LIN-41 T83, which is important for the

elimination of LIN-41 from embryos, are poor matches to this consensus sequence (sequence FDTPPSM, mismatches are underlined; Figure S10). The best match to a high-affinity CPD appears to be around residue T340 in the LIN-41 Deg-B2 domain (sequence LATPMSS; Figure S10). This was the only candidate Fbw7 binding site identified in LIN-41 using the Eukaryotic Linear Motif (ELM) database (Gouw *et al*. 2018), which requires a perfect match to a relatively stringent consensus sequence. However, changing T340 to an alanine (T340A) (e.g.: *lin-41(tn1541tn1775)* has no effect on the elimination of GFP::LIN-41 from embryos (Figure 2C and Figure S4, K and L). Therefore, if SEL-10 binds directly to LIN-41 Deg domains it might recognize imperfect or lower-affinity degrons. We note that the SEL-10 ortholog Cdc4p utilizes multiple imperfect degrons to target the cell division protein Sic1p for degradation (Nash *et al.* 2001). Likewise, multiple weak degrons in an intrinsically disordered region of the c-Jun protein synergize to promote a high-affinity interaction with the SEL-10 ortholog Fbw7 (Csizmok *et al*. 2018). It seems plausible that SEL-10 might function similarly. Alternatively, the failure to eliminate LIN-41 from embryos could be an indirect consequence of the lack of SCF^{SEL-10}. To begin to address this possibility, we sought to clarify the epistatic relationships between *sel-10* and other factors involved in the elimination of GFP::LIN-41 from embryos.

CDK-1 was previously shown to be required for the elimination of GFP::LIN-41 (Spike *et al*. 2014a). Likewise, *cdk-1(RNAi)* on *rrf-1(pk1417) lin-41(tn1541)* hermaphrodites prevents the elimination of GFP::LIN-41 from embryos (n=67; Figure S9, A and B). Therefore, germline-expressed CDK-1 likely promotes the elimination of GFP::LIN-41. CDK-1 is a conserved and essential cell-cycle regulator required for M-phase entry and progression during both meiotic and mitotic cell divisions (Boxem *et al*. 1999). Consequently, most *cdk-1* alleles are sterile,

761 precluding the examination of GFP::LIN-41 in *cdk-1* mutant embryos. Two temperature-
762 sensitive alleles of *cdk-1* that produce oocytes have been described; both cause a later
763 embryonic arrest phenotype than the 1-cell meiotic arrest phenotype seen after *cdk-1(RNAi)*
764 (Boxem *et al*. 1999; Shirayama *et al*. 2006). Furthermore, although both mutations alter
765 residues in the T loop/activation domain of CDK-1, neither *cdk-1(*ts*)* allele causes obvious cell-
766 cycle defects (Shirayama *et al*. 2006). We examined GFP::LIN-41 in *cdk-1(ne2257*ts*)* animals at
767 the restrictive temperature and found that GFP::LIN-41 disappears normally from embryos
768 (n=57; Figure S9, E and F). Similarly, GFP::LIN-41 disappears normally in *cks-1(ne549*ts*)* mutant
769 embryos (n=33; Figure S9, G and H), which phenotypically resemble *cdk-1(ne2257*ts*)* embryos
770 at the restrictive temperature (Shirayama *et al*. 2006). Thus, the subset of CDK-1 activities
771 affected by *cdk-1(ne2257*ts*)* does not include either the elimination of GFP::LIN-41 or entry into
772 meiotic M phase.

773 Kinases other than CDK-1 might play a role in the SEL-10-mediated elimination of LIN-
774 41. Indeed, WEE-1.3, a kinase that negatively regulates CDK-1 (Burrows *et al.* 2006), prevents
775 the premature elimination of GFP::LIN-41 from oocytes (Spike *et al*. 2014a). However, our
776 attempts to identify additional kinases that affect the elimination of GFP::LIN-41 have so far
777 been unsuccessful. For example, the mitogen-activated protein (MAP) kinase MPK-1 is active in
778 the late stages of oogenesis and is an important regulator of oocyte meiotic maturation (Lee *et*
779 *al*. 2007). Furthermore, as a proline-directed serine/threonine kinase, MPK-1 could potentially
780 phosphorylate CPDs in LIN-41 Deg domains. However, GFP::LIN-41 disappears normally in *mpk-*
781 *1(ga111*ts*)* embryos at the restrictive temperature (n=97; Figure S9, I–L). Likewise, the Aurora
782 kinase AIR-2 is present and active in maturing oocytes (Schumacher *et al*. 1998), but GFP::LIN-

41 is eliminated normally after *air-2* gene function is attenuated by *air-2(or207*ts*)* (n=14), by *air-2(RNAi)* (n=40), or after *air-2(RNAi)* on *air-2(or207*ts*)* mutants (n=38; Figure S9, M and N). Other single kinase knock-down or elimination experiments that have failed to affect the elimination of GFP::LIN-41 from *lin-41(tn1541)* embryos include *gsk-3(RNAi)* (n=32), *cdk-2(RNAi)* (n=24), *plk-1(RNAi)*, and *mbk-2(pk1427)* (Spike 2014a). Since LIN-41 functions to inhibit CDK-1 activation for M-phase entry during meiotic maturation (Spike *et al*. 2014a), CDK-1 may be the chief effector kinase mediating feedback regulation of wild-type LIN-41.

SEL-10/Fbw7/Cdc4p degrons are only activated after being phosphorylated by a proline-directed serine/threonine kinase such as CDK-1. Thus, prior phosphorylation by CDK-1 might be required for SEL-10 to directly interact with degrons in the LIN-41 Deg domains. *cdk-1(RNAi)* and *sel-10(lf)* cause the same phenotype with respect to GFP::LIN-41 degradation, precluding a direct analysis of their epistatic relationship. However, it is possible to examine this relationship indirectly through *wee-1.3* (Burrows *et al*. 2006). GFP::LIN-41 is eliminated prematurely when *wee-1.3* function is attenuated by RNAi; this occurs in both wild-type (Spike *et al*. 2014a) and *lon-3(e2175)* mutants (n=21; Figure 5, A and B). When the same experiment is performed in *lon-3(e2175) sel-10(ar41)* mutants, however, GFP::LIN-41 is not eliminated prematurely. Instead, GFP::LIN-41 persists, typically at reduced levels, in the proximal oocytes of *lon-3(e2175) sel-10(ar41); wee-1.3(RNAi)* animals (n=51; Figure 5, C and D). Because CDK-1 is prematurely activated, *wee-1.3(RNAi)* oocytes mature prematurely and exhibit numerous defects (Burrows *et al.* 2006). Obvious oocyte abnormalities caused by strong *wee-1.3(RNAi)* are evident in *sel-10(ar41)* mutants, confirming that these animals are competent to respond to *wee-1.3(RNAi)* (Figure 5, compare B and D). We conclude that the epistatic relationship

805 between *wee-1.3* and *sel-10* is consistent with the model shown in Figure 5E, which postulates
806 that active CDK-1 promotes the phosphorylation of LIN-41 and its subsequent destruction by an
807 SCF^{SEL-10} E3 ubiquitin ligase.

808

809 ***Embryonic LIN-41 does not strongly inhibit the expression of mRNAs repressed by LIN-41***

810 LIN-41 represses the translation of several different mRNAs during oogenesis (Spike *et al*.
811 2014b; Tsukamoto *et al*. 2017). Their protein products normally begin to accumulate in late
812 oogenesis or early embryogenesis, and some are essential for normal development (Gomes *et*
813 *al*. 2001; Leacock and Reinke 2008; Tsukamoto *et al.* 2017). We therefore anticipated that the
814 failure to eliminate LIN-41 would result in the ectopic repression of these mRNAs, and that this,
815 in turn, might result in embryo or oocyte abnormalities. However, the *lin-41(tn1767)* mutant,
816 which fails to eliminate LIN-41[T83A] from early embryos, appears essentially wild-type at 20°C
817 (Table 1). Similarly, *sel-10(ok1632)* and *sel-10(ar41)* mutants, which fail to eliminate LIN-41
818 from early embryos, produce large broods of progeny at 20°C that are similar in size to
819 genotype-matched controls (Table 3). Indeed, we only observed a moderate decrease in fertility
820 when *sel-10(ok1632)* mutants were grown at an elevated temperature (25°C; Table 3). We
821 therefore decided to examine the amount of protein made by several LIN-41 target mRNAs
822 (*spn-4*, *meg-1*, and *orc-1* mRNAs, respectively) in strains that fail to eliminate LIN-41 from
823 embryos, as this should provide a sensitive way to monitor LIN-41 translational repression
824 activity. Protein expression was examined using fluorescently-tagged alleles of each gene; the
825 proteins made by *spn-4(tn1699[spn-4::gfp::3xflag])*, *meg-1(tn1724[gfp::3xflag::meg-1])* and

826 *orc-1(tn1732[mng::3xflag::orc-1)* were previously shown to be ectopically or prematurely
827 expressed in *lin-41(lf)* oocytes (Tsukamoto *et al*. 2017). As described below, only minor
828 differences in protein expression were observed in *lin-41(tn1767)* and *sel-10(ar41)* embryos and
829 oocytes (Figure 6 and Figure S11). Collectively, these observations suggest that the ectopic LIN-
830 41 present in *lin-41(tn1767)* and *sel-10(lf)* embryos is largely ineffective at repressing
831 translation.

832 LIN-41 mediates 3'-UTR-dependent translational repression of *spn-4*, and *spn-4* mRNA is
833 the most abundant and enriched mRNA in LIN-41 RNPs (Tsukamoto *et al*. 2017). SPN-4::GFP is
834 faint, but visible, in 1 or 2 proximal oocytes and rapidly accumulates during the oocyte-to-
835 embryo transition (Tsukamoto *et al*. 2017). This pattern, and the amount of SPN-4::GFP in early
836 embryos, is largely unaffected by *lin-41(tn1767)* and *sel-10(ar41)* at 20°C (Figure 6, A, B, G, and
837 H, and Figure S11, A, B, K, and L). Quantification of GFP levels revealed no differences in SPN-
838 4::GFP levels in *lin-41(tn1767); spn-4(tn1699)* 1- and 2-cell embryos and a slight reduction in
839 SPN-4::GFP levels in *spn-4(tn1699) lon-3(e2175) sel-10(ar41)* 2-cell embryos relative to age and
840 genotype-matched controls (Figure 6, K and L). In these quantitative experiments, we analyzed
841 the anterior cytoplasm of 1- and 2-cell embryos and did not include the bright puncta of SPN-
842 4::GFP evident in the posterior cytoplasm (see Materials and Methods). Finally, we also failed to
843 identify any apparent differences in SPN-4::GFP accumulation or intensity in *spn-4(tn1699) lon-*
844 *3(e2175) sel-10(ar41)* (n=26) and *spn-4(tn1699) lon-3(e2175)* (n=19) animals upshifted as L4s to
845 25°C.

GFP::MEG-1 expression is evident somewhat earlier in oogenesis than SPN-4::GFP and seems to accumulate more slowly. Again, the pattern and amount of GFP::MEG-1 was largely unaffected in *lin-41(tn1767)* and *sel-10(ar41)* mutants at 20°C (Figure 6, C, D, I, and J, and Figure S11, C, D, G, and H). GFP::MEG-1 has a complex pattern of accumulation in the early embryo; it appears to be eliminated from somatic blastomeres and localizes, at least partially, to P granules (Figure 6C and Figure S11C), similar to what was previously described by Leacock and Reinke (2008) for endogenous MEG-1. Due to these complexities, we quantified GFP::MEG-1 levels in the cytoplasm of proximal oocytes instead of embryos. There were no differences in GFP::MEG-1 levels in *lin-41(tn1767); meg-1(tn1724)* animals and only a slight reduction in the –1 oocytes of *lon-3(e2175) sel-10(ar41); meg-1(tn1724)* animals relative to controls. Finally, we examined *lon-3(e2175) sel-10(ar41); meg-1(tn1724)* (n=17) and *lon-3(e2175); meg-1(tn1724)* (n=15) animals upshifted as L4s to 25°C, but again failed to identify any apparent differences in GFP::MEG-1 accumulation.

mNG::ORC-1 is not visibly expressed in oocytes but becomes increasingly evident in embryos as they develop (Tsukamoto *et al.* 2017). mNG::ORC-1 associates with chromatin at certain stages of the cell cycle (Sonneville *et al*. 2012), and is faintly visible in 1-cell embryos during metaphase of the first mitotic division (Figure 6E). mNG::ORC-1 was only examined in *lin-41(tn1767)* mutants at 20°C. As for SPN-4::GFP and GFP::MEG-1, the pattern and amount of mNG::ORC-1 was largely unaffected by *lin-41(tn1767)* (Figure 6, E and F, and Figure S11, E and F). Most importantly, the small amount of mNG::ORC-1 visible in 1-cell embryos was not obviously reduced in the *lin-41(tn1767)* background. Because LIN-41 is a potent translational repressor of *spn-4*, *meg-1*, and *orc-1* (Tsukamoto *et al*. 2017), we conclude that a mechanism

868 distinct from SCF^{SEL-10}-mediated degradation antagonizes LIN-41 function to promote their
869 expression during the late stages of oogenesis and the OET.

870 Because molecular tests failed to reveal an increase in LIN-41 activity in *sel-10* mutants,
871 we also tested the ability of a *sel-10(ok1632)* strong loss-of-function mutation to suppress the
872 temperature-sensitive *lin-41(tn1487*ts*)* allele at a semi-permissive temperature. This was found
873 not to be the case; rather, *sel-10(ok1632)* enhanced the *lin-41(tn1487*ts*)* defects (Table 3).
874 Taken together, these results indicate that the regulation of LIN-41 by *sel-10* is nonessential.

875

876 ***SEL-10 promotes the elimination of GLD-1 from oocytes***

877 GLD-1 is a translational repressor that, like LIN-41, controls and coordinates oocyte
878 differentiation and cell cycle progression (Francis *et al*. 1995a,b; Jones *et al*. 1996). In *gld-*
879 *1(q485)* null mutants, pachytene-stage oocytes re-enter the mitotic cell cycle and form a tumor
880 (Francis *et al*. 1995a,b). GLD-1 also has redundant functions to inhibit the proliferative fate of
881 germline progenitor cells and to promote their entry into the meiotic pathway of development
882 during oogenesis and spermatogenesis, as well as a function to promote spermatogenesis in
883 hermaphrodites (Francis *et al*. 1995a,b; Kadyk and Kimble 1998). GLD-1 is abundantly expressed
884 during the early and middle stages of meiotic prophase, but eliminated from oocytes as they
885 progress from late pachytene through diplotene and to diakinesis during the later stages of
886 oocyte development (Jones *et al*. 1996). GLD-1 binds to, and represses the translation of, many
887 mRNAs that are normally translated in oocytes (Lee and Schedl 2001; Lee and Schedl 2004;
888 Schumacher *et al*. 2005; Wright *et al*. 2011; Jungkamp *et al*. 2011; Scheckel *et al*. 2012). Thus, it

889 has generally been assumed that the elimination of GLD-1 from oocytes permits the translation
890 of these mRNAs (reviewed in Lee and Schedl 2010). Although it occurs at an earlier stage of
891 oocyte development, this model is analogous to what we originally hypothesized with respect
892 to LIN-41. However, because the LIN-41 ectopically found in *sel-10* loss-of-function embryos
893 appears to be insufficient to sustain translational repression, it seems likely that the activity of
894 LIN-41 is also regulated by a non-proteolytic mechanism. Given the similarities between LIN-41
895 and GLD-1, we wondered whether GLD-1 might also be regulated by both proteolytic and non-
896 proteolytic mechanisms.

897 To begin to approach this question, we investigated whether the elimination of GLD-1,
898 like LIN-41, requires SEL-10. Surprisingly, we found that GLD-1::GFP and GLD-1 do indeed
899 persist at elevated levels in the oocytes of *sel-10(ar41)* and *sel-10(ok1632)* mutants (Figure 7, A
900 and B, and Figure S12, A, B, D, and E), indicating that LIN-41 and GLD-1 may be regulated
901 similarly. Indeed, while we were completing this work, the failure to eliminate GLD-1 in a timely
902 fashion from *sel-10(ok1632)* mutant oocytes was independently discovered by Kisielnicka *et al*.
903 (2018). Their results suggest that both GLD-1 and the cytoplasmic polyadenylation element-
904 binding protein CPB-3 are likely degraded by essentially the same SCF^{SEL-10} E3 ubiquitin ligase
905 (Kisielnicka *et al.* 2018) that regulates LIN-41 (this work). Consistent with this hypothesis, they
906 observed that slow-migrating isoforms of GLD-1, which are likely phosphorylated (Jeong *et al*.
907 2011), accumulate in *sel-10(ok1632)* mutants. In agreement with this finding, we also observe
908 an increase in the slow-migrating isoforms of GLD-1 in both *sel-10(ok1632)* and *sel-10(ar41)*
909 mutants relative to controls (Figure 7C).

It was recently proposed that sperm trigger the proteasome-dependent elimination of GLD-1 from oocytes such that a GFP::GLD-1 transgene (an N-terminal fusion) was expressed at higher levels in unmated females than in mated females or hermaphrodites (Bohnert and Kenyon 2017). We therefore decided to examine the localization of a rescuing GLD-1::GFP transgene (a C-terminal fusion) in both wild-type and *sel-10(ar41)* mutant females, which lack sperm. However, in our experiments, GLD-1::GFP did not persist at elevated levels in female oocytes; instead, it was eliminated from oocytes in both the presence and absence of sperm (Figure 7, A and D, Figure S12, A and C). Likewise, endogenous GLD-1, detected with specific antibodies (Jan *et al*. 1999), also disappeared from oocytes in both hermaphrodites and females (Figure S12, D and F). However, GLD-1::GFP levels remained elevated in the oocytes of *sel-10(ar41)* mutant females (Figure 7E). Oocytes remain in the gonad for an extended period of time in the absence of sperm (McCarter *et al*. 1999). Indeed, we noticed that there seemed to be relatively less GLD-1::GFP in the s*el-10(ar41)* oocytes of females as compared to hermaphrodites, possibly as a result of *sel-10*-independent protein turnover. From these results, we conclude that the *sel-10*-dependent elimination of GLD-1::GFP is sperm-independent. Furthermore, the expression patterns of GLD-1::GFP, which rescues the *gld-1(q485)* null mutation to fertility (Schumacher *et al*. 2005; Figure 7A), and endogenous GLD-1 (Figure S12, D and F), fail to support the hypothesis that sperm trigger the elimination of GLD-1 from oocytes. We have tested the GFP::GLD-1 transgene (*axIs1498[pie-1p::gfp::gld-1::gld-1 3'UTR, unc-119(+)]*; Merritt *et al.* 2008) used by Bohnert and Kenyon (2017) to monitor GLD-1 expression in females; however, we found that it fails to rescue *gld-1(q485)* null mutants to fertility. Adult *gld-1(q485); axIs1498* hermaphrodites are invariably sterile and exhibit a range

of phenotypes from a tumorous phenotype that is equivalent to the null allele to the production of abnormal oocytes. We analyzed 192 progeny from *gld-1(q485)/+; axIs1498* adult hermaphrodites; 53 (27.6%) were *gld-1(q485); axIs1498* and were sterile, consistent with the inability of *axIs1498* to provide wild-type *gld-1* function. We conclude that the increased expression of GFP::GLD-1 observed in the oocytes of *axIs1498* females (Bohnert and Kenyon 2017) is most likely a transgene expression artifact and does not reflect the expression and regulation of endogenous GLD-1.

Ectopic GLD-1 in proximal oocytes does not strongly inhibit the expression of mRNAs repressed by GLD-1

As for LIN-41, we examined whether the mRNA targets of GLD-1-mediated translational repression are ectopically repressed in *sel-10(ar41)* mutant oocytes. Studies of GLD-1 function in the proliferative versus meiotic entry decision of germline progenitor cells demonstrate that GLP-1/Notch signaling functions to inhibit GLD-1 accumulation in the distal end of the germline. When GLD-1 accumulates ectopically in *glp-1* mutants, or double mutants affecting the Pumilio and FBF proteins FBF-1 and FBF-2, germline progenitor cells fail to proliferate and prematurely enter the meiotic pathway of development (Crittenden *et al*. 2002; Hansen *et al*. 2004). Thus, our initial expectation was that ectopic GLD-1 expression in proximal oocytes in strong *sel-10* loss-of-function mutants might exert substantial effects on the repression of its mRNA targets. As for LIN-41, this proved not to be the case; only subtle or modest effects were observed as described below.

GLD-1 binds the 3'-UTR of the *spn-4* mRNA (Junkamp *et al*. 2011), which we initially examined as a LIN-41 target, and GLD-1 appears to repress SPN-4 accumulation in the distal germline (Mootz *et al*. 2004). As described previously, SPN-4::GFP expression was not strongly affected by the *sel-10(ar41)* mutation (Figure S11, I–L) despite the ectopic expression of both GLD-1 and LIN-41 (Figure 4 and Figure 7). MEX-3 is expressed in proximal oocytes and also appears to be repressed by GLD-1 (Mootz *et al*. 2004; Jungkamp *et al.* 2011). We used the fluorescently-tagged *mex-3(tn1753[gfp::3xflag::mex-3])* allele to quantitatively examine the expression of GFP::MEX-3 in these oocytes at both 20° and 25°C. GFP::MEX-3 levels were not reduced in *sel-10(ar41)* oocytes at either temperature, but were generally very similar to the wild-type controls (Figure 7F, and Figure S12H). In addition, we examined the expression of the yolk receptor RME-2 (Grant and Hirsh 1999), a well-established target of GLD-1-mediated translational repression (Lee and Schedl 2001; Junkamp *et al*. 2011; Wright *et al.* 2011). We began by examining the expression of RME-2::GFP from *pwIs116[rme-2p::rme-2::GFP::rme-2 3'UTR]* in oocytes at 22°C, to prevent transgene silencing. Again, the levels of RME-2::GFP were similar in the proximal oocytes of *sel-10(ar41)* and wild-type controls (Figure 7, G and H). Likewise, similar levels of endogenous RME-2 were seen in *sel-10(ok1632)* and wild-type oocytes stained with anti-RME-2-specific antibodies (Figure S12, I and J). Finally, we examined the expression of OMA-2, another well-established target of GLD-1-mediated translational repression (Lee and Schedl 2004; Wright *et al*. 2011; Scheckel *et al*. 2012). As we examined the expression of mNG::OMA-2 in *sel-10(ar41)* embryos in our analysis of LIN-41 Deg domains (Figure S7, A–D; described above), we quantitatively compared the expression level of mNG::OMA-2 expression in the proximal oocytes of the wild type and *sel-10(ar41)* mutants and

observed a modest reduction (~30–50%) in mNG::OMA-2 expression levels in *sel-10(ar41)* mutants (Figure 7I). This result is agreement with the finding that an antibody that detects OMA-2 and its paralog OMA-1 exhibits a modest reduction in immuofluoresence staining (~10-33%, depending on the region of the proximal gonad analyzed) in the *sel-10(ok1632*) strong loss-of-function mutant (Kisielnicka *et al.* 2018).

Collectively, these results suggest that the ectopic GLD-1 in *sel-10* mutant oocytes is minimally effective at repressing translation of mRNA targets. The observation that some targets (e.g., *spn-4*, *mex-3*, and *rme-2*) might be unaffected by ectopic GLD-1, whereas others (e.g., *oma-2*) are modestly affected, is consistent with the observation that certain *gld-1* mutant alleles disrupt binding and repression of some mRNA targets but not others (Schumacher *et al*. 2005). Furthermore, these observations are again consistent with the fact that *sel-10* mutants are viable and fertile (Table 3), as the efficient repression of proteins such as SPN-4, MEX-3 and RME-2 during oogenesis should have negative consequences for embryonic development (Draper *et al.* 1996; Grant and Hirsh 1999; Gomes *et al*. 2001).

The SCF^{SEL-10}-dependent degradation of LIN-41 and GLD-1 depend on different kinases

As described above, the SCF^{SEL-10}-dependent degradation of LIN-41 depends on CDK-1, but not MPK-1 (Figure S9, I–L). Consequently, we examined the requirement of these kinases for the SCF^{SEL-10}-dependent degradation of GLD-1. Whereas *cdk-1(RNAi)* or *cdk-2(RNAi)* had no effect on the accumulation of GLD-1::GFP in proximal oocytes (n=14 and n=23, respectively), we observed ectopic expression of GLD-1::GFP in the proximal oocytes of *ozIs5[gld-1::gfp]; mpk-*

1(ga111ts) hermaphrodites at the non-permissive temperature (Figure S13). Thus, although both GLD-1 and LIN-41 are regulated by SCF^{SEL-10}-dependent degradation, the temporal and spatial control of their accumulation during oogenesis is differentially responsive to protein kinase signaling, befitting their individual biological functions in promoting oogenesis.

DISCUSSION

Feedback regulation of LIN-41 and the spatial control of oocyte meiotic maturation

The oocytes of most sexually reproducing animals arrest in meiotic prophase for a prolonged period (reviewed by Huelgas-Morales and Greenstein 2017; Avilés-Pagán and Orr-Weaver 2018). This conserved arrest likely enables transcriptionally quiescent oocytes to grow by accumulating cellular organelles and cytoplasmic factors needed for embryonic development. Indeed, in *C. elegans* oocyte growth and meiotic maturation are coordinately controlled by LIN-41. In the absence of LIN-41 function, pachytene-stage oocytes abruptly cellularize, activate CDK-1, and enter M phase (Spike *et al*. 2014a). A salient feature of *C. elegans* oogenesis is that meiotic maturation is restricted to the oocyte in the most proximal position adjacent the spermatheca. This restriction ensures that only fully grown oocytes undergo meiotic maturation when they are positioned to enter the spermatheca during ovulation so they can become fertilized. Genetic evidence suggests that OMA proteins function to inhibit LIN-41 to facilitate meiotic maturation of the most proximal oocyte (Spike *et al*. 2014a). Specifically, proximal oocytes fail to enter M phase in *lin-41(*ts*); oma-1(null); oma-2(null)* triple mutants; whereas, pachytene stage oocytes prematurely enter M phase in *lin-41(null); oma-1(null); oma-2(null)* triple mutants (Spike *et al.* 2014a). Thus, the OMA proteins are absolutely required to spatially restrict for M-phase entry to the –1 oocyte, where they counteract LIN-41's inhibitory activity. Consistent with this idea, molecular evidence suggests that LIN-41 is inactivated as a translational repressor in the final stages of oogenesis (Spike *et al*. 2014a; Tsukamoto *et al*. 2017), which precedes the elimination of LIN-41 upon the onset of meiotic maturation.

Specifically, two targets of LIN-41-mediated translational repression, *spn-4* and *meg-1*, are co-expressed with LIN-41 in the most proximal oocytes. The expression of *spn-4* and *meg-1* in proximal oocytes requires the function of the OMA proteins (Tsukamoto *et al.* 2017), consistent with the idea that the OMA proteins antagonize LIN-41 function in the late stages of oogenesis.

Here we show that the SCF^{SEL-10} promotes the rapid ubiquitin-mediated degradation of LIN-41 that leads to its elimination during meiosis I. Analysis of *sel-10* mutants indicates that the inactivation and degradation of LIN-41 are separable; the LIN-41 that accumulates in *sel-10* mutants appears to be largely inactive as a translational repressor. However, we did note that several LIN-41 variants (LIN-41(T83A) and LIN-41(ΔDeg-A)), which are defective in the SCF^{SEL-10}-mediated degradation, decrease the meiotic maturation rate. This finding is consistent with the idea that LIN-41 inhibits meiotic maturation and that SCF^{SEL-10}-mediated degradation constitutes a non-essential component of the regulatory mechanism. The nature of the "primary" mechanism inactivating LIN-41 prior to its degradation is currently unknown but could act on LIN-41 directly or another component of the large RNP complex it associates with (Spike *et al*. 2014b; Tsukamoto *et al*. 2017).

LIN-41 and CDK-1 reciprocally inhibit one another's activity. Thus, the "primary" inactivation mechanism might play a key role in tipping the balance between LIN-41 and CDK-1 to generate a spatially restricted all-or-none meiotic maturation response. Upon its activation, CDK-1 triggers meiotic maturation and promotes the SCF^{SEL-10}-dependent elimination of LIN-41. The elimination of LIN-41 requires the Deg-A and Deg-B domains in the LIN-41 N-terminal region. The LIN-41 Deg-A and Deg-B domains are intrinsically disordered and contain

sequences that might function as phosphodegrons. The SCF^{SEL-10}-dependent elimination of LIN-41 is blocked by the T83A mutation affecting a predicted CDK-1 phosphorylation site within the Deg-A domain, though whether this regulation is direct or indirect remains to be determined. We note one exception to the rule that CDK-1 activity promotes LIN-41 degradation. The *lin-41(tn1541tn1618)* mutation (Figure 2), which deletes the NHL domain, produces a strong loss-of-function *lin-41* mutant phenotype in which pachytene-stage oocytes enter M phase precociously. Nonetheless, we observe that the GFP::LIN-41(ΔNHL) protein still accumulates in the proximal gonad, albeit in an aberrantly punctate pattern (Figure S3, G–J). Interestingly, in the presence of a wild-type LIN-41 protein, the GFP::LIN-41(ΔNHL) mutant protein accumulates normally and is subject to SCF^{SEL-10}-dependent degradation on schedule. It may be that the accumulation of the GFP::LIN-41(ΔNHL) protein in a punctate pattern correlates with its inaccessibility to CDK-1-dependent regulation. Alternatively, the degradation of LIN-41 during meiotic maturation may depend on LIN-41 activity during pachytene, as could be the case if a component of the SCF^{SEL-10} degradation mechanism depends on *lin-41* function for its synthesis or activity.

The Deg domains may function as a timer to ensure that CDK-1 activity reaches an optimal threshold to ensure the successful completion of the meiotic divisions prior to the initiation of LIN-41 degradation. If LIN-41 is eliminated too early the fidelity of meiotic chromosome segregation may be compromised as is observed in certain hypomorphic *lin-41* mutant alleles (e.g., *tn1487tn1515*, *tn1487tn1516*, *tn1487tn1536*, and *tn1487tn1539*; Spike *et al.* 2014a). Thus, it will be important to elucidate the precise mechanisms by which the LIN-41 Deg domains link CDK-1 activity to SCF^{SEL-10}-mediated degradation. The regulation of the G1/S

phase transition in budding yeast provides a framework for thinking about this issue (Nash *et al*. 2001; Kõvomägi *et al*. 2011; Yang *et al*. 2013; reviewed by Hopkins *et al*. 2017). The cyclin-dependent kinase complex, Cdk1–Clb5/6 promotes the entry into S phase but is inhibited by binding to its inhibitor Sic1 (Nugroho and Mendenhall 1994; Schwob *et al.* 1994). Sic1 is a substrate of the Cdk1–Clb5/6 kinase, which phosphorylates Sic1 to promote SCF^{Cdc4}-mediated degradation (Verma *et al*. 1997; Feldman *et al*. 1997; Nash *et al*. 2001). The cyclin-dependent kinase Cdk1–Cln1/2 initiates the decision to enter S phase during G1 and is not inhibited by Sic1. Phosphorylation of Sic1 by Cdk1–Cln1/2, while not sufficient to trigger Sic1 degradation, primes Sic1 for multisite phosphorylation by Clb5/6. The Sic1 CPD sequences contain multiple sites for phosphorylation by both Cdk1–Clb5/6 and Cdk1–Cln1/2, which results in the switch-like destruction of Sic1. A failure to degrade Sic1 substantially delays the G1/S transition, whereas deletion of SIC1 causes DNA replication to initiate too early, resulting in genome instability (Nugroho *et al*. 1994; Cross *et al*. 2007). Further dissection of the mechanism by which the LIN-41 Deg domains function will illuminate whether analogous mechanisms are employed in a developmental context.

Ubiquitin-mediated protein degradation and the OET

Signaling pathways and downstream kinase activation coordinate the cell-cycle and developmental events that underpin oocyte and early embryo development. In *C. elegans* the ERK MAP kinase signaling pathway and its effector kinase MPK-1 regulate pachytene progression and multiple aspects of oogenesis, including oocyte growth and specific events that

occur during meiotic maturation (reviewed by Arur 2017). Consistent with these phenotypes, sustained activation of MPK-1 occurs during pachytene and in proximal oocytes (Lee *et al*. 2007). Likewise, in proximal oocytes activated cyclin-dependent kinase CDK-1 regulates an important aspect of oocyte meiotic maturation by promoting the transition from meiotic prophase to meiotic M phase, as we have described. Once activated, CDK-1 phosphorylates the DYRK mini-brain kinase MBK-2 as part of an intricate regulatory mechanism that permits MBK-2 activation near the end of the first meiotic division (Pellettieri *et al*. 2003; Stitzel *et al.* 2006, 2007; Cheng *et al*. 2009; Parry *et al*. 2009). These three kinases (MPK-1, CDK-1, and MBK-2) all function, at least in part, to promote the degradation of one or more RNA-binding proteins during oogenesis or the OET.

After meiosis, the OMA proteins are detectably phosphorylated by activated MBK-2 (Nishi and Lin 2005). Phosphorylation by MBK-2 promotes a direct physical interaction between the OMA proteins and the transcription factor TAF-4; this permits the sequestration of TAF-4 in the cytoplasm and prevents the premature onset of zygotic transcription (Guven-Ozkan *et al.* 2008). Furthermore, MBK-2-dependent phosphorylation primes the OMA proteins for phosphorylation by the glycogen synthase kinase GSK-3 and for degradation during the first mitotic division (Nishi and Lin, 2005; Shirayama *et al.* 2006). In addition to MBK-2 and GSK-3, the degradation of the OMA proteins requires the normal activities of additional kinases, including CDK-1/Cyclin B3, and several proposed E3 ubiquitin ligases (Shirayama *et al*. 2006; Du *et al*. 2015). The failure to degrade OMA-1 and eliminate it from early embryos is deleterious (Lin *et al.* 2003) and contributes to phenotypes exhibited by mutants that fail to degrade the OMA proteins (Shirayama *et al.* 2006). Indeed, the ectopic expression of OMA-1 in early

1108 embryos represses the translation of at least one mRNA target of the OMA proteins, *zif-1*
1109 mRNA, but only when OMA-1 is not phosphorylated by MBK-2, as in the *oma-1(zu405*gf*)*
1110 mutant (Guven-Ozkan *et al.* 2010). Thus, the MBK-2-dependent phosphorylation of the OMA
1111 proteins not only primes these proteins for degradation but also inhibits their ability to function
1112 as translational repressors.

1113 Likewise, the ability of GLD-1 to function as a translational repressor might be inhibited
1114 by MPK-1-dependent phosphorylation (Kisielnicka *et al.* 2018; this work). Since *mpk-1* activity is
1115 also required for the elimination of GLD-1, MPK-1-dependent phosphorylation would
1116 coordinate the inactivation of GLD-1 as a translational repressor with GLD-1 degradation.
1117 Consistent with this hypothesis, MPK-1 promotes the phosphorylation of GLD-1 and promotes
1118 its SCF^{SEL-10}-mediated degradation (Kisielnicka *et al.* 2018; this work). Furthermore, this
1119 hypothesis potentially explains why the ectopic GLD-1 expressed in *sel-10* mutant oocytes is
1120 relatively ineffective at repressing the translation of multiple target mRNAs.

1121 In sharp contrast to OMA-1 and GLD-1, our current understanding of the regulation of
1122 LIN-41 suggests that the inactivation of LIN-41 as a translational repressor is temporally and
1123 molecularly distinct from its degradation. Targets of LIN-41 translational repression such as *spn-*
1124 *4* and *meg-1* are actively translated prior to meiotic maturation and the CDK-1-dependent
1125 elimination of LIN-41. We have not yet determined that LIN-41 is phosphorylated by CDK-1 or
1126 any other kinase, as electrophoretic mobility changes are not reproducibly observed in *sel-10*
1127 mutants using several gel systems (unpublished results). The fact that *spn-4* and *meg-1* mRNAs
1128 are translated normally when *cdk-1* function is attenuated by RNAi (Tsukamoto *et al.* 2018)

suggests that the CDK-1 is not required to inactivate LIN-41 as a translational repressor. In addition, we show here that mutations affecting the function of the LIN-41 Deg domains do not exhibit gain-of-function phenotypes or substantially repress the translation of LIN-41 target mRNAs.

Multiple mechanisms regulate LIN-41 proteins

LIN-41 was first identified through its role in the heterochronic gene regulatory pathway that controls the timing of postembryonic cell divisions and cell fate decisions in somatic cells in *C. elegans* (Reinhart *et al*. 2000; Slack *et al*. 2000; reviewed by Rougvie and Moss 2013). In this capacity, LIN-41 functions to repress the translation of several transcription factors, including LIN-29, MAB-3, MAB-10, and DMD-3, which play key roles in specifying somatic cell fates during the L4 and adult stages (Reinhart *et al*. 2000; Harris and Horvitz 2011; Aeschimann *et al*. 2017). LIN-41 binds to the mRNAs of these genes and represses their translation during early larval stages (e.g., L1–L3) (Aeschimann *et al*. 2017). The Let-7 microRNA promotes the switch from early larval stages to the L4 and adult stages by repressing translation of LIN-41 beginning in the L4 stage (Reinhart *et al*. 2000; Slack *et al*. 2000). This regulation is specific to the soma as the *let-7(n2583*ts*)* mutation does not increase the accumulation of LIN-41 in the oogenic germline (Spike *et al*. 2014a). It is not clear whether specific protein degradation mechanisms collaborate with Let-7-mediated regulation to ensure that LIN-41 does not perdure from the early larval stages into the L4 and adult stage in somatic cells. If such mechanisms exist, they are unlikely to depend solely on the Deg domains because *lin-41* mutations affecting the Deg domains (e.g.,

tn1620, *tn1622 tn1635*, *tn1638*, *tn1643*, and *tn1645*) do not phenocopy *let-7* mutations or exhibit dominant somatic defects. Additionally, the Deg mutations do not confer an overt *lin-41(lf)* Dpy phenotype. Further, *lin-41(tn1541tn1643[ΔDeg-A–RING–Deg-B])* L3-stage larvae do not exhibit precocious adult alae (n=7; Ann Rougvie, personal communication) as is frequently observed in *lin-41(n2914)* null mutants (Slack *et al*. 2000). The Deg domains mediate LIN-41 degradation during the OET over short time scales (i.e., 10–15 minutes), whereas the larval stages last for hours. This difference may obviate a requirement for SCF^{SEL-10}-mediated degradation of LIN-41 during the larval stages. Interestingly, several *lin-41* gain-of-function alleles affecting the N-terminal 39 amino acid residues result in a defect in tip retraction during male tail development resulting in the production of a leptoderan (Lep) tail characteristic of other rhabditid nematode species (Del Rio-Albrechtsen *et al*. 2006). These *lin-41(Lep)* gain-of-function alleles do not affect LIN-41 degradation during the OET and thus define a site for LIN-41 regulation in somatic cells, which could involve proteolytic degradation.

LIN-41 is highly conserved. The mammalian ortholog LIN-41/TRIM71 is required for embryonic viability and neural tube closure in mice (Maller Schulman *et al*. 2008; Cuevas *et al*. 2015; Mitschka *et al*. 2015). LIN-41/TRIM71 was found to promote reprogramming of dermal fibroblasts to induced-pluripotent stem cells (IPSC) through the negative regulation of differentiation genes including the transcription factor EGR1 (Worringer *et al*. 2014). Importantly, the Let-7 microRNA inhibits reprogramming in part through the repression of LIN-41. Thus, the regulation of LIN-41 by Let-7 is a conserved regulatory module. By contrast, the Deg domains of *C. elegans* LIN-41 are not found in the mammalian orthologs and appear to be rapidly evolving in closely related rhabditid nematodes.

Developing systems must deploy mechanisms to extinguish RNA-binding protein-mediated translational repression. Such mechanisms may function to promote translation of batteries of genes needed to drive developmental transitions. LIN-41-associated mRNAs include many key genes required for embryonic development (Tsukamoto *et al*. 2017). Thus the inactivation of LIN-41 likely plays a key role in shaping the proteome during the OET. The "primary" mechanism inactivating LIN-41 prior to its degradation, and its potential conservation in LIN-41 orthologs or members of the TRIM-NHL class of RNA-binding proteins, remain to be determined.

ACKNOWLEDGMENTS

We are grateful to Swathi Arur, Sarah Crittenden, Claire de la Cova, Daniel Dickinson, Bob Goldstein, Barth Grant, Iva Greenwald, Judith Kimble, Tim Schedl, and Dustin Updike for providing strains or reagents. We thank G. W. Gant Luxton for the use of his spinning disc confocal microscope. Some strains were provided by the Caenorhabditis Genetics Center, which is funded by grant P40OD010440 from the NIH Office of Research Infrastructure Programs. We also thank WormBase for sequences and annotations. We thank Cynthia Kenyon for discussions on GLD-1 regulation. Ann Rougvie and Todd Starich provided helpful suggestions during the course of this work. This work was supported by NIH grant GM57173 (to D.G.).

REFERENCES

Aeschimann, F., P. Kumari, H. Bartake, D. Gaidatzis, L. Xu *et al.*, 2017 LIN41 post-transcriptionally silences mRNAs by two distinct and position-dependent mechanisms. Mol. Cell 65**:** 476–489.

Allen, A. K., J. E. Nesmith, and A. Golden, 2014 An RNAi-based suppressor screen identifies interactors of the Myt1 ortholog *of Caenorhabditis elegans*. G3 4: 2329–2343.

Arribere, J. A., R. T. Bell, B. X. Fu, K. L. Artiles, P. S. Hartman *et al.*, 2014 Efficient marker-free recovery of custom genetic modifications with CRISPR/Cas9 in *Caenorhabditis elegans*. Genetics 198**:** 837–846.

Arur, S., 2017 Signaling-mediated regulation of meiotic prophase I and transition during oogenesis. Results Probl. Cell Differ. 59: 101–123.

Avilés-Pagán, E. E., and T. L. Orr-Weaver, 2018 Activating embryonic development in *Drosophila*. Semin. Cell Dev. Biol. in press.

Balklava, Z., S. Pant, H. Fares, and B. D. Grant, 2007 Genome-wide analysis identifies a general requirement for polarity proteins in endocytic traffic. Nat. Cell Biol. 9**:** 1066–1073.

Barroca, V., B. Lassalle, M. Coureuil, J. P. Louis, F. Le Page *et al.*, 2009 Mouse differentiating spermatogonia can generate germinal stem cells *in vivo*. Nat. Cell Biol. 11: 190–196.

Beard, S. M., R. B. Smit, B. G. Chan, and P. E. Mains, 2016 Regulation of the MEI-1/MEI-2 microtubule-severing Katanin complex in early *Caenorhabditis elegans* Development. G3 6**:** 3257–3268.

Boag, P. R., A. Nakamura, and T. K. Blackwell, 2005 A conserved RNA-protein complex component involved in physiological germline apoptosis regulation in *C. elegans*.

Development 132: 4975–4986.

Bohnert, K. A., and C. Kenyon, 2017 A lysosomal switch triggers proteostasis renewal in the immortal *C. elegans* germ lineage. Nature 551**:** 629–633.

Boxem, M., D. G. Srinivasan, and S. van den Heuvel, 1999 The *Caenorhabditis elegans* gene *ncc-1* encodes a cdc2-related kinase required for M phase in meiotic and mitotic cell divisions, but not for S phase. Development 126**:** 2227–2239.

Brawley, C., and E. Matunis, 2004 Regeneration of male germline stem cells by spermatogonial dedifferentiation *in vivo*. Science 304: 1331–1334.

Burrows, A. E., B. K. Sceurman, M. E. Kosinski, C. T. Richie, P. L. Sadler *et al.*, 2006 The *C. elegans* Myt1 ortholog is required for the proper timing of oocyte maturation. Development 133**:** 697–709.

Castilho, P. V., B. C. Williams, S., Mochida, Y. Zhao, and M. L. Goldberg, 2009 The M phase kinase Greatwall (Gwl) promotes inactivation of PP2A/B55delta, a phosphatase directed against CDK phosphosites. Mol. Biol. Cell 20: 4777–4789.

Cheng, J., N. Türkel, N. Hemati, M. T. Fuller, A. J. Hunt, and Y. M. Yamashita, 2008 Centrosome misorientation reduces stem cell division during aging. Nature 456: 599–604.

Cheng, K. C., R. Klancer, A. Singson, and G. Seydoux, 2009 Regulation of MBK-2/DYRK by CDK-1 and the pseudophosphatases EGG-4 and EGG-5 during the oocyte-to-embryo transition. Cell 139**:** 560–572.

Crittenden, S. L., D. S. Bernstein, J. L. Bachorik, B. E. Thompson, M. Gallegos *et al.*, 2002 A conserved RNA-binding protein controls germline stem cells in *Caenorhabditis elegans*. Nature 417**:** 660–663.

1235 Cross, F. R., L. Schroeder, and J. M. Bean, 2007 Phosphorylation of the Sic1 inhibitor of B-type
1236 cyclins in *Saccharomyces cerevisiae* is not essential but contributes to cell cycle
1237 robustness. Genetics 176: 1541–1555.
1238 Csizmok, V., M. Montecchio, H. Lin, M. Tyers, M. Sunnerhagen *et al.*, 2018 Multivalent
1239 interactions with Fbw7 and Pin1 facilitate recognition of c-Jun by the SCF^{Fbw7} ubiquitin
1240 ligase. Structure 26: 28–39.
1241 Cuevas, E., A. Rybak-Wolf, A. M. Rhode, D. T. T. Nguyen, and F. G. Wulczyn, 2015 Lin41/Trim71
1242 is essential for mouse development and specifically expressed in postnatal ependymal
1243 cells of the brain. Front. Cell Dev. Biol. 3: 20.

1244 de la Cova, C., and I. Greenwald, 2012 SEL-10/Fbw7-dependent negative feedback regulation of
1245 LIN-45/Braf signaling in *C. elegans* via a conserved phosphodegron. Genes Dev 26**:**
1246 2524–2535.
1247 Del Rio-Albrechtsen, T., K. Kiontke, S. Y. Chiou, and D. H. Fitch, 2006 Novel gain-of-function
1248 alleles demonstrate a role for the heterochronic gene *lin-41* in *C. elegans* male tail tip
1249 morphogenesis. Dev. Biol. 297**:** 74–86.
1250 Dephoure, N., K. L. Gould, S. P. Gygi, and D. R. Kellogg, 2013 Mapping and analysis of
1251 phosphorylation sites: a quick guide for cell biologists. Mol. Biol. Cell 24**:** 535-542.
1252 Deshaies, R. J., and J. E. Ferrell, 2001 Multisite phosphorylation and the countdown to S phase.
1253 Cell 107**:** 819–822.
1254 Detwiler, M. R., M. Reuben, X. Li, E. Rogers, and R. Lin, 2001 Two zinc finger proteins, OMA-1
1255 and OMA-2, are redundantly required for oocyte maturation in *C. elegans*. Dev. Cell 1**:**
1256 187–199.

1257 Dickinson, D. J., A. M. Pani, J. K. Heppert, C. D. Higgins, and B. Goldstein, 2015 Streamlined
1258 genome engineering with a self-excising drug selection cassette. Genetics 200**:** 1035–
1259 1049.
1260 Dickinson, D. J., J. D. Ward, D. J. Reiner, and B. Goldstein, 2013 Engineering the *Caenorhabditis*
1261 *elegans* genome using Cas9-triggered homologous recombination. Nat. Methods 10**:**
1262 1028–1034.
1263 Doh, J. H., Y. Jung, V. Reinke, and M. H. Lee, 2013 *C. elegans* RNA-binding protein GLD-1
1264 recognizes its multiple targets using sequence, context, and structural information to
1265 repress translation. Worm 2: e26548.
1266 Draper, B. W., C. C. Mello, B. Bowerman, J. Hardin, and J. R. Priess, 1996 MEX-3 is a KH domain
1267 protein that regulates blastomere identity in early *C. elegans* embryos. Cell 87**:** 205–216.
1268 Du, Z., F. He, Z. Yu, B. Bowerman, and Z. Bao, 2015 E3 ubiquitin ligases promote progression of
1269 differentiation during *C. elegans* embryogenesis. Dev. Biol. 398**:** 267–279.
1270 Dunphy, W. G., L. Brizuela, D. Beach, and J. Newport, 1988 The *Xenopus* cdc2 protein is a
1271 component of MPF, a cytoplasmic regulator of mitosis. Cell 54**:** 423–431.
1272 Esposito, D., M. G. Koliopoulos, and K. Rittinger, 2017 Structural determinants of TRIM protein
1273 function. Biochem. Soc. Trans. 45**:** 183-191.
1274 Farley, B. M., and S. P. Ryder, 2012 POS-1 and GLD-1 repress *glp-1* translation through a
1275 conserved binding-site cluster. Mol. Biol. Cell 23**:** 4473–4483.
1276 Ferrell, J. E., Jr., 1999a *Xenopus* oocyte maturation: new lessons from a good egg. Bioessays 21:
1277 833–842.
1278 Ferrell, J. E., Jr., 1999b Building a cellular switch: more lessons from a good egg. Bioessays 21:

866–870.

Feldman, R. M., C. C. Correll, K. B. Kaplan, and R. J. Deshaies, 1997 A complex of Cdc4p, Skp1p, and Cdc53/cullin catalyzes ubiquitination of the phosphorylated CDK inhibitor Sic1p. Cell 91: 221–230.

Félix, M.-A., and A. Wagner 2008 Robustness and evolution: concepts, insights and challenges from a developmental model system. Heredity 100: 132–140.

Fox, P. M., V. E. Vought, M. Hanazawa, M. H. Lee, E. M. Maine *et al.*, 2011 Cyclin E and CDK-2 regulate proliferative cell fate and cell cycle progression in the *C. elegans* germline. Development 138**:** 2223–2234.

Francis, R., M. K. Barton, J. Kimble, and T. Schedl, 1995a *gld-1*, a tumor suppressor gene required for oocyte development in *Caenorhabditis elegans*. Genetics 139**:** 579–606.

Francis, R., E. Maine, and T. Schedl, 1995b Analysis of the multiple roles of *gld-1* in germline development: interactions with the sex determination cascade and the *glp-1* signaling pathway. Genetics 139**:** 607–630.

Frank-Vaillant, M., C. Jessus, R. Ozon, J. L. Maller, and O. Haccard, 1999 Two distinct mechanisms control the accumulation of cyclin B1 and Mos in *Xenopus* oocytes in response to progesterone. Mol. Biol. Cell 10**:** 3279–3288.

Furuta, T., S. Tuck, J. Kirchner, B. Koch, R. Auty *et al.*, 2000 EMB-30: an APC4 homologue required for metaphase-to-anaphase transitions during meiosis and mitosis in *Caenorhabditis elegans*. Mol. Biol. Cell 11**:** 1401–1419.

Gautier, J., C. Norbury, M. Lohka, P. Nurse, and J. Maller, 1988 Purified maturation-promoting factor contains the product of a *Xenopus* homolog of the fission yeast cell cycle control

gene cdc2+. Cell 54**:** 433–439.

Gautier, J., J. Minshull, M. Lohka, M. Glotzer, T. Hunt *et al.*, 1990 Cyclin is a component of maturation-promoting factor from *Xenopus*. Cell 60**:** 487–494.

Gomes, J. E., S. E. Encalada, K. A. Swan, C. A. Shelton, J. C. Carter *et al.*, 2001 The maternal gene *spn-4* encodes a predicted RRM protein required for mitotic spindle orientation and cell fate patterning in early *C. elegans* embryos. Development 128**:** 4301–4314.

Gouw, M., S. Michael, H. Sámano-Sánchez, M. Kumar, A. Zeke *et al.*, 2018 The eukaryotic linear motif resource - 2018 update. Nucleic Acids Res. 46**:** D428–D434.

Govindan, J. A., H. Cheng, J. E. Harris, and D. Greenstein, 2006 Galphao/i and Galphas signaling function in parallel with the MSP/Eph receptor to control meiotic diapause in *C. elegans*. Curr. Biol. 16**:** 1257–1268.

Govindan, J. A., S. Nadarajan, S. Kim, T. A. Starich, and D. Greenstein, 2009 Somatic cAMP signaling regulates MSP-dependent oocyte growth and meiotic maturation in *C. elegans*. Development 136**:** 2211–2221.

Grant, B., and D. Hirsh, 1999 Receptor-mediated endocytosis in the *Caenorhabditis elegans* oocyte. Mol. Biol. Cell 10**:** 4311–4326.

Guven-Ozkan, T., Y. Nishi, S. M. Robertson, and R. Lin, 2008 Global transcriptional repression in *C. elegans* germline precursors by regulated sequestration of TAF-4. Cell 135**:** 149–160.

Haccard, O., and C. Jessus, 2006a Redundant pathways for Cdc2 activation in *Xenopus* oocyte: either cyclin B or Mos synthesis. EMBO Rep. 7: 321–325.

Haccard, O., and C. Jessus, 2006b Oocyte maturation, Mos and cyclins–a mater of synthesis: two functionally redundant ways to induce meiotic maturation. Cell Cycle 5: 1152–1159.

1323 Hammerstein, P., E. H. Hagen, A. V. M. Hertz, and H. Herzel, 2006 Robustness: a key to
1324 evolutionary design. Biological Theory 1: 90–93.
1325 Hansen, D., L. Wilson-Berry, T. Dang, and T. Schedl, 2004 Control of the proliferation versus
1326 meiotic development decision in the *C. elegans* germline through regulation of GLD-1
1327 protein accumulation. Development 131**:** 93–104.
1328 Harris, D. T., and H. R. Horvitz, 2011 MAB-10/NAB acts with LIN-29/EGR to regulate terminal
1329 differentiation and the transition from larva to adult in *C. elegans*. Development 138:
1330 4051–4062.

1331 Hasegawa, E., T. Karashima, E. Sumiyoshi, and M. Yamamoto, 2006 *C. elegans* CPB-3 interacts
1332 with DAZ-1 and functions in multiple steps in germline development. Dev. Biol. 295:
1333 689–699.

1334 Huelgas-Morales, G., and D. Greenstein, 2017 Control of oocyte meiotic maturation in *C.*
1335 *elegans*. Semin. Cell Dev. Biol., in press.

1336 Hopkins, M., J. J. Tyson, and B. Novák, 2017 Cell-cycle transitions: a common role for
1337 stoichiometric inhibitors. Mol. Biol. Cell 28: 3437–3446.
1338 Hsu, J. Y., Z. W. Sun, X. Li, M. Reuben, K. Tatchell *et al.*, 2000 Mitotic phosphorylation of histone
1339 H3 is governed by Ipl1/aurora kinase and Glc7/PP1 phosphatase in budding yeast and
1340 nematodes. Cell 102**:** 279–291.
1341 Ikeda, K., and S. Inoue, 2012 TRIM proteins as RING finger E3 ubiquitin ligases. Adv. Exp. Med.
1342 Biol. 770**:** 27–37.
1343 Jan, E., C. K. Motzny, L. E. Graves, and E. B. Goodwin, 1999 The STAR protein, GLD-1, is a

translational regulator of sexual identity in *Caenorhabditis elegans*. EMBO J. 18**:** 258–269.

Jeong, J., J. M. Verheyden, and J. Kimble, 2011 Cyclin E and Cdk2 control GLD-1, the mitosis/meiosis decision, and germline stem cells in *Caenorhabditis elegans*. PLoS Genet. 7**:** e1001348.

Jones, A. R., R. Francis, and T. Schedl, 1996 GLD-1, a cytoplasmic protein essential for oocyte differentiation, shows stage- and sex-specific expression during *Caenorhabditis elegans* germline development. Dev. Biol. 180**:** 165–183.

Jones, A. R., and T. Schedl, 1995 Mutations in *gld-1*, a female germ cell-specific tumor suppressor gene in *Caenorhabditis elegans*, affect a conserved domain also found in Src-associated protein Sam68. Genes Dev. 9**:** 1491–1504.

Jungkamp, A. C., M. Stoeckius, D. Mecenas, D. Grün, G. Mastrobuoni *et al.*, 2011 *In vivo* and transcriptome-wide identification of RNA binding protein target sites. Mol. Cell 44**:** 828–840.

Jäger, S., H. T. Schwartz, H. R. Horvitz, and B. Conradt, 2004 The *Caenorhabditis elegans* F-box protein SEL-10 promotes female development and may target FEM-1 and FEM-3 for degradation by the proteasome. Proc. Natl. Acad. Sci. U S A 101**:** 12549–12554.

Kadyk, L. C., and J. Kimble, 1998 Genetic regulation of entry into meiosis in *Caenorhabditis elegans*. Development 125**:** 1803–1813.

Kai, T., and Spradling A., 2004 Differentiating germ cells can revert into functional stem cells in *Drosophila melanogaster* ovaries. Nature 428: 564–569.

Kapelle, W. S., and V. Reinke, 2011 *C. elegans meg-1* and *meg*-2 differentially interact with

1366 nanos family members to either promote or inhibit germ cell proliferation and survival.
1367 Genesis 49: 380–391.
1368 Killian, D. J., E. Harvey, P. Johnson, M. Otori, S. Mitani *et al.*, 2008 SKR-1, a homolog of Skp1 and
1369 a member of the SCF(SEL-10) complex, regulates sex-determination and LIN-12/Notch
1370 signaling in *C. elegans*. Dev. Biol. 322**:** 322–331.
1371 Kim, M. Y., E. Bucciarelli, D. G. Morton, B. C. Williams, K. Blake-Hodek *et al*., 2012 Bypassing the
1372 Greatwall-Endosulfine pathway: plasticity of a pivotal cell-cycle regulatory module in
1373 *Drosophila* and *Caenorhabditis elega*ns. Genetics 191: 1181–1197.
1374 Kipreos, E. T., S. P. Gohel, and E. M. Hedgecock, 2000 The *C. elegans* F-box/WD-repeat protein
1375 LIN-23 functions to limit cell division during development. Development 127**:** 5071–
1376 5082.
1377 Kipreos, E. T., L. E. Lander, J. P. Wing, W. W. He, and E. M. Hedgecock, 1996 *cul-1* is required for
1378 cell cycle exit in *C. elegans* and identifies a novel gene family. Cell 85**:** 829–839.
1379 Kishimoto, T., 2015 Entry into mitosis: a solution to the decades-long enigma of MPF.
1380 Chromosoma 124**:** 417–428.
1381 Kisielnicka, E., R. Minasaki, and C. R. Eckmann, 2018 MAPK signaling couples SCF-mediated
1382 degradation of translational regulators to oocyte meiotic progression. Proc. Natl. Acad.
1383 Sci. U S A 115**:** E2772–E2781.
1384 Kobayashi, H., J. Minshull, C. Ford, R. Golsteyn, R. Poon *et al.*, 1991 On the synthesis and
1385 destruction of A- and B-type cyclins during oogenesis and meiotic maturation in *Xenopus*
1386 *laevis*. J. Cell Biol. 114**:** 755–765.
1387 Kõivomägi, M., E. Valk, R. Venta, A. Iofik, M. Lepiku *et al.*, 2011 Cascades of multisite

phosphorylation control Sic1 destruction at the onset of S phase. Nature 480: 128–131.

Kornbluth, S., B. Sebastian, T. Hunter, and J. Newport, 1994 Membrane localization of the kinase which phosphorylates p34cdc2 on threonine 14. Mol. Biol. Cell 5: 273–282.

Kosinski, M., K. McDonald, J. Schwartz, I. Yamamoto, and D. Greenstein, 2005 *C. elegans* sperm bud vesicles to deliver a meiotic maturation signal to distant oocytes. Development 132: 3357–3369.

Kumagai, A., and W. G. Dunphy, 1996 Purification and molecular cloning of Plx1, a Cdc25-regulatory kinase from *Xenopus* egg extracts. Science 273:1377–1380.

Kumari, P., F. Aeschimann, D. Gaidatzis, J. J. Keusch, P. Ghosh *et al.*, 2018 Evolutionary plasticity of the NHL domain underlies distinct solutions to RNA recognition. Nat. Commun. 9**:** 1549.

Kumsta, C., and M. Hansen, 2012 *C. elegans rrf-1* mutations maintain RNAi efficiency in the soma in addition to the germline. PLoS One 7**:** e35428.

Leacock, S. W., and V. Reinke, 2008 MEG-1 and MEG-2 are embryo-specific P-granule components required for germline development in *Caenorhabditis elegans*. Genetics 178**:** 295–306.

Lee, M. H., M. Ohmachi, S. Arur, S. Nayak, R. Francis *et al.*, 2007 Multiple functions and dynamic activation of MPK-1 extracellular signal-regulated kinase signaling in *Caenorhabditis elegans* germline development. Genetics 177**:** 2039–2062.

Lee, M. H., and T. Schedl, 2001 Identification of in vivo mRNA targets of GLD-1, a maxi-KH motif containing protein required for *C. elegans* germ cell development. Genes Dev. 15**:** 2408–2420.

1410 Lee, M. H., and T. Schedl, 2004 Translation repression by GLD-1 protects its mRNA targets from
1411 nonsense-mediated mRNA decay in *C. elegans*. Genes Dev. 18**:** 1047–1059.
1412 Lee, M. H., and T. Schedl, 2010 *C. elegans* star proteins, GLD-1 and ASD-2, regulate specific RNA
1413 targets to control development. Adv. Exp. Med. Biol. 693**:** 106–122.
1414 Li, W., L. R. DeBella, T. Guven-Ozkan, R. Lin, and L. S. Rose, 2009 An eIF4E-binding protein
1415 regulates katanin protein levels in *C. elegans* embryos. J. Cell Biol. 187**:** 33–42.
1416 Lin, R., 2003 A gain-of-function mutation in *oma-1*, a *C. elegans* gene required for oocyte
1417 maturation, results in delayed degradation of maternal proteins and embryonic
1418 lethality. Dev. Biol. 258**:** 226–239.
1419 Loedige, I., D. Gaidatzis, R. Sack, G. Meister, and W. Filipowicz, 2013 The mammalian TRIM-NHL
1420 protein TRIM71/LIN-41 is a repressor of mRNA function. Nucleic Acids Res. 41**:** 518–532.
1421 Loedige, I., L. Jakob, T. Treiber, D. Ray, M. Stotz *et al.*, 2015 The crystal structure of the NHL
1422 domain in complex with RNA reveals the molecular basis of *Drosophila brain-tumor*-
1423 mediated gene regulation. Cell Rep. 13**:** 1206–1220.
1424 Lohka, M. J., M. K. Hayes, and J. L. Maller, 1988 Purification of maturation-promoting factor, an
1425 intracellular regulator of early mitotic events. Proc. Natl. Acad. Sci. U S A 85**:** 3009–3013.
1426 Lucas, X., and A. Ciulli, 2017 Recognition of substrate degrons by E3 ubiquitin ligases and
1427 modulation by small-molecule mimicry strategies. Curr. Opin. Struct. Biol. 44**:** 101–110.
1428 Maller Schulman, B. R., X. Liang, C. Stahlhut, C. DelConte, G. Stefani *et al*., 2008 The *let-7*
1429 microRNA target gene, *Mlin41/Trim71* is required for mouse embryonic survival and
1430 neural tube closure. Cell Cycle 7: 3935–3942.
1431 Masui, Y., 2001 From oocyte maturation to the *in vitro* cell cycle: the history of discoveries of

1432 Maturation-Promoting Factor (MPF) and Cytostatic Factor (CSF). Differentiation 69: 1–
1433 17.

1434 Masui, Y., and C. L. Markert, 1971 Cytoplasmic control of nuclear behavior during meiotic
1435 maturation of frog oocytes. J. Exp. Zool. 177: 129–145.

1436 Matsuura, R., T. Ashikawa, Y. Nozaki, and D. Kitagawa, 2016 LIN-41 inactivation leads to delayed
1437 centrosome elimination and abnormal chromosome behavior during female meiosis in
1438 *Caenorhabditis elegans*. Mol. Biol. Cell 27: 799–811.

1439 McCarter, J., B. Bartlett, T. Dang, and T. Schedl, 1999 On the control of oocyte meiotic
1440 maturation and ovulation in *Caenorhabditis elegans*. Dev. Biol. 205: 111–128.

1441 McNally, K., A. Audhya, K. Oegema, and F. J. McNally, 2006 Katanin controls mitotic and meiotic
1442 spindle length. J. Cell Biol. 175: 881–891.

1443 Merritt, C., D. Rasoloson, D. Ko and, G. Seydoux, 2008 3' UTRs are the primary regulators of
1444 gene expression in the *C. elegans* germline. Curr. Biol. 18: 1476–1482.

1445 Miller, M. A., V. Q. Nguyen, M. H. Lee, M. Kosinski, T. Schedl *et al.*, 2001 A sperm cytoskeletal
1446 protein that signals oocyte meiotic maturation and ovulation. Science 291: 2144–2147.

1447 Minshull, J., A. Murray, A. Colman, and T. Hunt, 1991 *Xenopus* oocyte maturation does not
1448 require new cyclin synthesis. J. Cell Biol. 114: 767–772.

1449 Mitschka, S., T. Ulas, T. Goller, K. Schneider, A. Egert *et al*., 2015 Co-existence of intact stemness
1450 and priming of neural differentiation programs in mES cells lacking Trim71. Sci. Rep. 5:
1451 11126.

1452 Mochida, S., S. L. Maslen, M. Skehel, and T. Hunt, 2010 Greatwall phosphorylates an inhibitor of
1453 protein phosphatase 2A that is essential for mitosis. Science 330:1670–1673.

1454 Mohammad, A., K. Vanden Broek, C. Wang, A. Daryabeigi, V. Jantsch *et al.*, 2018 Initiation of
1455 meiotic development Is controlled by three posttranscriptional pathways in
1456 *Caenorhabditis elegans*. Genetics in press.
1457 Mootz, D., D. M. Ho, and C. P. Hunter, 2004 The STAR/Maxi-KH domain protein GLD-1 mediates
1458 a developmental switch in the translational control of *C. elegans* PAL-1. Development
1459 131**:** 3263–3272.
1460 Mueller, P. R., T. R. Coleman, and W. G. Dunphy, 1995 Cell cycle regulation of a *Xenopus* Wee1-
1461 like kinase. Mol Biol Cell 6: 119–134.Murray, A. W., M. J. Solomon, and M. W. Kirschner,
1462 1989 The role of cyclin synthesis and degradation in the control of maturation
1463 promoting factor activity. Nature 339**:** 280–286.
1464 Nakagawa, T., M. Sharma, Y. Nabeshima, R. E. Braun, and S. Yoshida, 2010 Functional hierarchy
1465 and reversibility within the murine spermatogenic stem cell compartment. Science 328:
1466 62–67.
1467 Nakagawa, T., Y. Nabeshima, and S. Yoshida, 2007 Functional identification of the actual and
1468 potential stem cell compartments in mouse spermatogenesis. Dev. Cell 12: 195–206.
1469 Nakayama, K. I., and K. Nakayama, 2005 Regulation of the cell cycle by SCF-type ubiquitin
1470 ligases. Semin. Cell Dev. Biol. 16**:** 323–333.
1471 Nash, P., X. Tang, S. Orlicky, Q. Chen, F. B. Gertler *et al.*, 2001 Multisite phosphorylation of a
1472 CDK inhibitor sets a threshold for the onset of DNA replication. Nature 414**:** 514–521.
1473 Nayak, S., F. E. Santiago, H. Jin, D. Lin, T. Schedl *et al.*, 2002 The *Caenorhabditis elegans* Skp1-
1474 related gene family: diverse functions in cell proliferation, morphogenesis, and meiosis.
1475 Curr. Biol. 12**:** 277–287.

1476 Nebreda, A. R., J. V. Gannon, and T. Hunt, 1995 Newly synthesized protein(s) must associate
1477 with p34cdc2 to activate MAP kinase and MPF during progesterone-induced maturation
1478 of Xenopus oocytes. EMBO J. 14**:** 5597–5607.
1479 Nishi, Y., and R. Lin, 2005 DYRK2 and GSK-3 phosphorylate and promote the timely degradation
1480 of OMA-1, a key regulator of the oocyte-to-embryo transition in *C. elegans*. Dev. Biol.
1481 288**:** 139–149.
1482 Nugroho, T. T., and M. D. Mendenhall, 1994 An inhibitor of yeast cyclin-dependent protein
1483 kinase plays an important role in ensuring the genomic integrity of daughter cells. Mol.
1484 Cell. Biol. 14: 3320–3328.
1485 Nurse, P., 1990 Universal control mechanism regulating onset of M-phase. Nature 344**:** 503–
1486 508.
1487 Nyström, J., Z. Z. Shen, M. Aili, A. J. Flemming, A. Leroi *et al.*, 2002 Increased or decreased levels
1488 of *Caenorhabditis elegans lon-3*, a gene encoding a collagen, cause reciprocal changes in
1489 body length. Genetics 161**:** 83–97.
1490 O'Farrell, P. H., 2001 Triggering the all-or-nothing switch into mitosis. Trends Cell Biol. 11**:** 512–
1491 519.
1492 Ogura, K., N. Kishimoto, S. Mitani, K. Gengyo-Ando, and Y. Kohara, 2003 Translational control of
1493 maternal *glp-1* mRNA by POS-1 and its interacting protein SPN-4 in *Caenorhabditis*
1494 *elegans*. Development 130**:** 2495–2503.
1495 Parry, J. M., N. V. Velarde, A. J. Lefkovith, M. H. Zegarek, J. S. Hang *et al.*, 2009 EGG-4 and EGG-5
1496 link events of the oocyte-to-embryo transition with meiotic progression in *C. elegans*.
1497 Curr. Biol. 19**:** 1752–1757.

1498 Peel, N., M. Dougherty, J. Goeres, Y. Liu, and K. F. O'Connell, 2012 The *C. elegans* F-box proteins
1499 LIN-23 and SEL-10 antagonize centrosome duplication by regulating ZYG-1 levels. J. Cell
1500 Sci. 125**:** 3535–3544.
1501 Pellettieri, J., V. Reinke, S. K. Kim, and G. Seydoux, 2003 Coordinate activation of maternal
1502 protein degradation during the egg-to-embryo transition in *C. elegans*. Dev. Cell 5**:** 451–
1503 462.
1504 Prince, V. E., and F. B. Pickett, 2002 Splitting pairs: the diverging fates of duplicated genes. Nat.
1505 Rev. Genet. 3: 827–837.
1506 Reinhart, B. J., F. J. Slack, M. Basson, A. E. Pasquinelli, J. C. Bettinger *et al.*, 2000 The 21-
1507 nucleotide *let-7* RNA regulates developmental timing in *Caenorhabditis elegans*. Nature
1508 403: 901–906.
1509 Robertson, S., and R. Lin, 2015 The maternal-to-zygotic transition in *C. elegans*. Curr. Top. Dev.
1510 Biol. 113**:** 1–42.
1511 Rose, K. L., V. P. Winfrey, L. H. Hoffman, D. H. Hall, T. Furuta *et al.*, 1997 The POU gene *ceh-18*
1512 promotes gonadal sheath cell differentiation and function required for meiotic
1513 maturation and ovulation in *Caenorhabditis elegans*. Dev. Biol. 192**:** 59–77.
1514 Rougvie, A. E., and E. G. Moss, 2013 Developmental transitions in *C. elegans* larval stages. Curr.
1515 Top. Dev. Biol. 105: 153–180,
1516 Rybak, A., H. Fuchs, K. Hadian, L. Smirnova, E. A. Wulczyn *et al.*, 2009 The *let-7* target gene
1517 mouse *lin-41* is a stem cell specific E3 ubiquitin ligase for the miRNA pathway protein
1518 Ago2. Nat. Cell. Biol. 11**:** 1411–1420.
1519 Scheckel, C., D. Gaidatzis, J. E. Wright, and R. Ciosk, 2012 Genome-wide analysis of GLD-1-

mediated mRNA regulation suggests a role in mRNA storage. PLoS Genet. 8**:** e1002742.

Schumacher, B., M. Hanazawa, M. H. Lee, S. Nayak, K. Volkmann *et al.*, 2005 Translational repression of *C. elegans* p53 by GLD-1 regulates DNA damage-induced apoptosis. Cell 120**:** 357–368.

Schumacher, J. M., A. Golden, and P. J. Donovan, 1998 AIR-2: An Aurora/Ipl1-related protein kinase associated with chromosomes and midbody microtubules is required for polar body extrusion and cytokinesis in *Caenorhabditis elegans* embryos. J. Cell Biol. 143**:** 1635–1646.

Shirayama, M., M. C. Soto, T. Ishidate, S. Kim, K. Nakamura *et al.*, 2006 The conserved kinases CDK-1, GSK-3, KIN-19, and MBK-2 promote OMA-1 destruction to regulate the oocyte-to-embryo transition in *C. elegans*. Curr. Biol. 16**:** 47–55.

Schwob, E., T. Böhm, M. D. Mendenhall, and K. Nasmyth, 1994 The B-type cyclin kinase inhibitor $p40^{SIC1}$ controls the G1 to S transition in *S. cerevisae*. Cell 79: 233–244.

Sijen, T., J. Fleenor, F. Simmer, K. L. Thijssen, S. Parrish *et al.*, 2001 On the role of RNA amplification in dsRNA-triggered gene silencing. Cell 107**:** 465–476.

Slack, F. J., M. Basson, Z. Liu, V. Ambros, H. R. Horvitz *et al.*, 2000 The *lin-41* RBCC gene acts in the *C. elegans* heterochronic pathway between the *let*-7 regulatory RNA and the LIN-29 transcription factor. Mol. Cell 5**:** 659–669.

Slack, F. J., and G. Ruvkun, 1998 A novel repeat domain that is often associated with RING finger and B-box motifs. Trends Biochem. Sci. 23**:** 474–475.

Sonneville, R., M. Querenet, A. Craig, A. Gartner, and J. J. Blow, 2012 The dynamics of replication licensing in live *Caenorhabditis elegans* embryos. J. Cell Biol. 196**:** 233–246.

1542 Spike, C. A., D. Coetzee, C. Eichten, X. Wang, D. Hansen *et al.*, 2014a The TRIM-NHL protein LIN-
1543 41 and the OMA RNA-binding proteins antagonistically control the prophase-to-
1544 metaphase transition and growth of *Caenorhabditis elegans* oocytes. Genetics 198**:**
1545 1535–1558.
1546 Spike, C. A., D. Coetzee, Y. Nishi, T. Guven-Ozkan, M. Oldenbroek *et al.*, 2014b Translational
1547 control of the oogenic program by components of OMA ribonucleoprotein particles in
1548 *Caenorhabditis elegans*. Genetics 198**:** 1513–1533.
1549 Stitzel, M. L., K. C. Cheng, and G. Seydoux, 2007 Regulation of MBK-2/Dyrk kinase by dynamic
1550 cortical anchoring during the oocyte-to-zygote transition. Curr. Biol. 17**:** 1545–1554.
1551 Stitzel, M. L., J. Pellettieri, and G. Seydoux, 2006 The *C. elegans* DYRK kinase MBK-2 marks
1552 oocyte proteins for degradation in response to meiotic maturation. Curr. Biol. 16**:** 56–
1553 62.
1554 Suzuki, Y., G. A. Morris, M. Han, and W. B. Wood, 2002 A cuticle collagen encoded by the *lon-3*
1555 gene may be a target of TGF-beta signaling in determining *Caenorhabditis elegans* body
1556 shape. Genetics 162**:** 1631–1639.
1557 Svoboda, P., H. Fulka, and R. Malik, 2017 Clearance of parental products. Adv. Exp. Med. Biol.
1558 953**:** 489–535.
1559 Timmons, L., and A. Fire, 1998 Specific interference by ingested dsRNA. Nature 395**:** 854.
1560 Tocchini, C., J. J. Keusch, S. B. Miller, S. Finger, H. Gut *et al.*, 2014 The TRIM-NHL protein LIN-41
1561 controls the onset of developmental plasticity in *Caenorhabditis elegans*. PLoS Genet.
1562 10**:** e1004533.
1563 Tsukamoto, T., M. D. Gearhart, C. A. Spike, G. Huelgas-Morales, M. Mews *et al.*, 2017 LIN-41

and OMA ribonucleoprotein complexes mediate a translational repression-to-activation switch controlling oocyte meiotic maturation and the oocyte-to-embryo transition in *Caenorhabditis elegans*. Genetics 206**:** 2007–2039.

Ubersax, J. A., E. L. Woodbury, P. N. Quang, M. Paraz, J. D. Blethrow *et al.*, 2003 Targets of the cyclin-dependent kinase Cdk1. Nature 425**:** 859–864.

van der Voet, M., M. A. Lorson, D. G. Srinivasan, K. L. Bennett, and S. van den Heuvel, 2009 *C. elegans* mitotic cyclins have distinct as well as overlapping functions in chromosome segregation. Cell Cycle 8: 4091–4102.

Vavouri, T., J. I. Semple, and B. Lehner, 2008 Widespread conservation of genetic redundancy during a billion years of eukaryotic evolution. Trends Genet. 24: 485–488.

Verlhac, M. H., M. E. Terret, and L. Pintard, 2010 Control of the oocyte-to-embryo transition by the ubiquitin-proteolytic system in mouse and *C. elegans*. Curr. Opin. Cell Biol. 22**:** 758–763.

Verma, R., R. S. Annan, M. J. Huddleston, S. A. Carr, G. Reynard *et al*., 1997 Phosphorylation of Sic1p by G_1 Cdk required for its degradation and entry into S phase. Science 278: 455–460.

Von Stetina, J. R., S. Tranguch, S. K. Dey, L. A. Lee, B. Cha *et al*., 2008) alpha-Endosulfine is a conserved protein required for oocyte meiotic maturation in *Drosophila*. Development 135: 3697–3706.

Wang, J. T., J. Smith, B. C. Chen, H. Schmidt, D. Rasoloson *et al*., 2014 Regulation of RNA granule dynamics by phosphorylation of serine-rich, intrinsically disordered proteins in *C. elegans*. Elife 3: e04591.

1586 Welcker, M., and B. E. Clurman, 2008 FBW7 ubiquitin ligase: a tumour suppressor at the
1587 crossroads of cell division, growth and differentiation. Nat Rev Cancer 8**:** 83–93.
1588 Wolke, U., E. A. Jezuit, and J. R. Priess, 2007 Actin-dependent cytoplasmic streaming in *C.*
1589 *elegans* oogenesis. Development 134**:** 2227–2236.
1590 Wright, J. E., D. Gaidatzis, M. Senften, B. M. Farley, E. Westhof *et al.*, 2011 A quantitative RNA
1591 code for mRNA target selection by the germline fate determinant GLD-1. EMBO J. 30**:**
1592 533–545.
1593 Worringer, K. A., T. A. Rand, Y. Hayashi, S. Sami, K. Takahashi *et al.*, 2014 The *let*-7/LIN-41
1594 pathway regulates reprogramming to human induced pluripotent stem cells by
1595 controlling expression of prodifferentiation genes. Cell Stem Cell 14: 40–52.
1596 Yamanaka, A., M. Yada, H. Imaki, M. Koga, Y. Ohshima *et al.*, 2002 Multiple Skp1-related
1597 proteins in *Caenorhabditis elegans*: diverse patterns of interaction with Cullins and F-
1598 box proteins. Curr. Biol. 12**:** 267–275.
1599 Yang, X., K.–Y. Lau, V. Sevim, and C. Tang, 2013 Design principles of the yeast G1/S switch. PLoS
1600 Biol. 11: e1001673.
1601 Yu, J., Y. Zhao, Z. Li, S. Galas, and M. L. Goldberg, 2006 Greatwall kinase participates in the Cdc2
1602 autoregulatory loop in *Xenopus* egg extracts. Mol Cell 22: 83–91.
1603 Zhao, Y., O. Haccard, R. Wang, J. Yu, J. Kuang *et al*., 2008 Roles of Greatwall kinase in the
1604 regulation of cdc25 phosphatase. Mol. Biol. Cell 19: 1317–1327.
1605

1606 **TABLES**

1607 **Table 1 Fertility and fecundity of *lin-41* alleles at 20°C**

GENOTYPE	PREDICTED PROTEIN CHANGE	FERTILE (%)[a]	BROOD SIZE[b]	DEAD EMBRYOS (%)[c]
lin-41(tn1541)	N-terminal GFP	100 (n=68)	316 ± 39[d] (n=6)	0.3 (n=361)
lin-41(tn1541tn1618)[e,f]	Δ NHL (AA 819-1128)	1.5 (n=65)	1 (n=1)	ND
lin-41(tn1541tn1571)[e,f]	Δ Ig (AA 677-824)	78.5 (n=65)	11 ± 12 (n=9)	57.1[g] (n=35)
lin-41(tn1541tn1562)[e,f]	Δ Bbox-CC (AA 356-707)[h]	84 (n=87)	6 ± 3 (n=17)	ND
lin-41(tn1541tn1643)[e]	Δ N-terminal (AA 40-356)	66 (n=90)	6 ± 4 (n=48)	75.4[g] (n=142)
lin-41(tn1541tn1620)[e]	Δ N-terminal (AA 40-205)	97 (n=67)	39 ± 32 (n=10)	36.4[g] (n=110)
lin-41(tn1541tn1622)[e]	Δ Deg-B2 (AA 206-356)	100 (n=65)	33 ± 16 (n=6)	39.0[g] (n=105)
lin-41(tn1541tn1635)	Δ Deg-B1 (AA 162-205)	100 (n=70)	127 ± 108 (n=10)	2.9 (n=105)
lin-41(tn1541tn1630)	Δ RING	98.5	210 ± 87	2.8

	(AA 113-161)	(n=65)	(n=12)	(n=144)
lin-41(tn1541tn1638)	Δ Deg-A	100	217 ± 103	6.3
	(AA 40-112)	(n=70)	(n=10)	(n=174)
lin-41(tn1541tn1645)	T83A	100	251 ± 86	1.0
		(n=70)	(n=10)	(n=193)
lin-41(tn1767)	T83A	98.3	313 ± 31	0.0
		(n=120)	(n=6)	(n=176)

[a] Fertile animals produced at least 1 viable offspring.

[b] The average number of progeny that hatched from fertile animals ± the standard deviation.

[c] The percent lethality among the embryos laid on Day 1 of adulthood.

[d] Essentially identical to the *lin-41(tn1541)* brood size previously reported in Spike *et al*. 2014 (319 ± 28 (n=30)).

[e] The progeny of *lin-41/hT2[qIs48]* hermaphrodites.

[f] These animals have a dumpy (Dpy) body shape, as previously described for *lin-41(lf)* alleles (Slack *et al*. 2000).

[g] Some of the embryos laid were small or otherwise appeared to be abnormal.

[h] The minimum number of amino acids removed by *tn1562*. Assuming the use of an in-frame 5' splice site in the 17-bp insertion, either one amino acid (L) or five amino acids (LSPLL) would replace amino acids 356-707.

Table 2 Sterility and embryonic lethality in *oma-2* and *oma-1; oma-2* mutant strains at 20°C

Genotype	Embryos laid[a]	Dead embryos (%)
oma-2(cp145)	314 ± 48 (n=6)	0.6 (n=1793)
oma-2(tn1760)	306 ± 39 (n=6)	0.6 (n=1835)
oma-2(tn1764)	300 ± 45 (n=6)	2.1 (n=1797)
oma-2(tn1764) lon-3(e2175) sel-10(ar41)	288 ± 26 (n=6)	1.1 (n=1727)
oma-1(zu405te33)	261 ± 18 (n=6)	0.8 (n=1568)
oma-1(zu405te33); oma-2(te51) M+Z-[b]	0 (n>21)[c]	NA
oma-1(zu405te33); oma-2(cp145)	212 ± 29 (n=12)	12.3[d] (n=2516)
oma-1(zu405te33); oma-2(tn1760)	224 ± 35 (n=6)	60.3 (n=1341)
oma-1(zu405te33); oma-2(tn1764) M+Z–[b,e]	249 ± 29 (n=5)	100 (n>1256)
oma-1(zu405te33); oma-2(tn1764) lon-3(e2175) sel-10(ar41) M+Z–[b,f]	246 ± 32 (n=6)	89.4 (n=1476)
oma-1(zu405te33); oma-2(tn1764) lon-3(e2175) sel-10(ar41)	196 ± 56 (n=6)	84.9 (n=1175)

[a] Average number of embryos laid per worm ± standard deviation.

[b] M+Z– animals were the progeny of *nT1[qIs51]* balancer-containing parents, which are heterozygous for both *oma-1* and *oma-2*. All other animals were the progeny of parents of the listed genotype.

[c] Sterile, with a defect in meiotic maturation as described by Detwiler *et al*. 2001.

[d] Percent embryo lethality was variable among the 12 parents analyzed; it ranged between 6 and 35%.

[e] These animals lay many eggs, none of which hatch (n=30).

[f] These animals lay many eggs, some of which hatch (n=24).

1633 **Table 3 *sel-10* mutant brood sizes at 20° and 25°C**

GENOTYPE	T (°C)	BROOD SIZE
wild type	20	304.0 ± 31.1 (n=29)
wild type[a]	25	266.8 ± 39.0 (n=19)
sel-10(ok1632)[a]	20	258.3 ± 67.7 (n=30)
sel-10(ok1632)[a]	25	72.2 ± 34.0[b] (n=30)
*lin-41(tn1487*ts); *sel-10(ok1632)*[c]	20	3.2 ± 3.4 (n=53)
*lin-41(tn1487*ts)[d]	20	41.4 ± 23.8 (n=36)
lon-3(e2175)	20	294.5 ± 36.7 (n=20)
lon-3(e2175) sel-10(ar41)	20	280.2 ± 40.1 (n=20)

1634 [a] Newly fertilized embryos were collected at 15°C and shifted to 25°C.

1635 [b] Approximately 10.0 ± 5.3% of *sel-10(ok1632*) hermaphrodites (n=3568)
1636 are infertile, exhibiting incompletely penetrant sterility or maternal-effect
1637 lethality when grown and examined for seven generations at 25°C.

1638 [c] The progeny of *sel-10(ok1632); lin-41(tn1487*ts*)/hT2[qIs48]*
1639 hermaphrodites.

1640 [d] The progeny of *lin-41(tn1487*ts*)/hT2(qIs48)* hermaphrodites.

1641

1642

1643

1644

1645 **FIGURE LEGENDS**

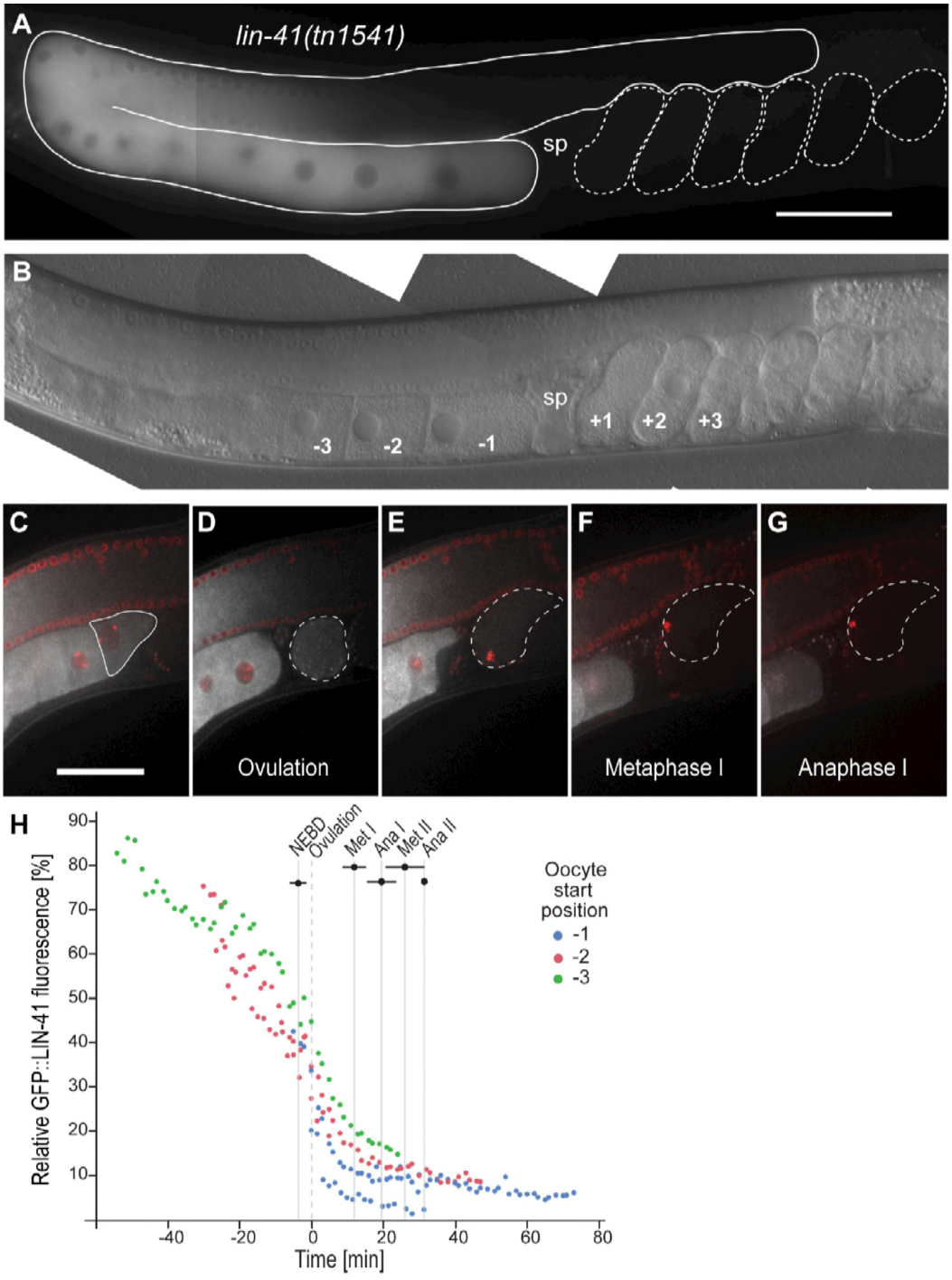

1646

1647 FIGURE 1. GFP::LIN-41 is eliminated during the first meiotic division. (A, B) Composite GFP (A)

1648 and DIC (B) images of a *lin-41(tn1541[gfp::tev::s-tag::lin-41])* adult hermaphrodite. GFP::LIN-41

is apparent in the middle and proximal regions of the germline (solid outline, (A)), with reduced levels in the –1 oocyte immediately adjacent to the spermatheca (sp). The positions of some embryos (dashed outlines, (A)) and oocytes are indicated relative to the spermatheca in (B); a fertilized embryo in the spermatheca would be at the zero position. These labels and naming conventions are used throughout. 100 ms GFP exposures; scale bar, 50 μm. (C–G) Time-lapse images of GFP::LIN-41 (white) and mCHERRY::HISTONE-labeled chromosomes (red) were acquired in a living *lin-41(tn1541); itIs37[pie-1p::mCherry:::H2B::pie-1 3'UTR, unc-119(+)]* adult hermaphrodite by confocal microscopy. Images are shown for select time points (*t*) prior to meiotic maturation (C, *t*=–4.5 min), at ovulation (D, *t*=0 min), and during the first meiotic division (E, *t*=+4 min; F, *t*=+11.8 min; G, *t*=+16.9 min) as an individual oocyte (C, solid outline) progresses from the –1 to the +1 position and through the OET (D–G, dashed outlines). Scale bar, 50 μm. Movie S1, worm #1, shows the complete time-lapse series from which the still images were taken. (H) Five oocytes were imaged as they progressed from the –1 position through meiotic divisions; the relative amount of background-corrected GFP::LIN-41 with respect to distal oocytes is shown on the graph at each time point. Three of the oocytes were also imaged at earlier stages as they moved from a more distal location (–2 oocyte (red) or –3 oocyte (green) position) into the –1 oocyte position (blue), as indicated. Timing on the *x*-axis is relative to ovulation (*t*=0). Bars indicate the standard deviation for different meiotic events (e.g.: NEBD, nuclear envelope breakdown; Met, metaphase; Ana, anaphase).

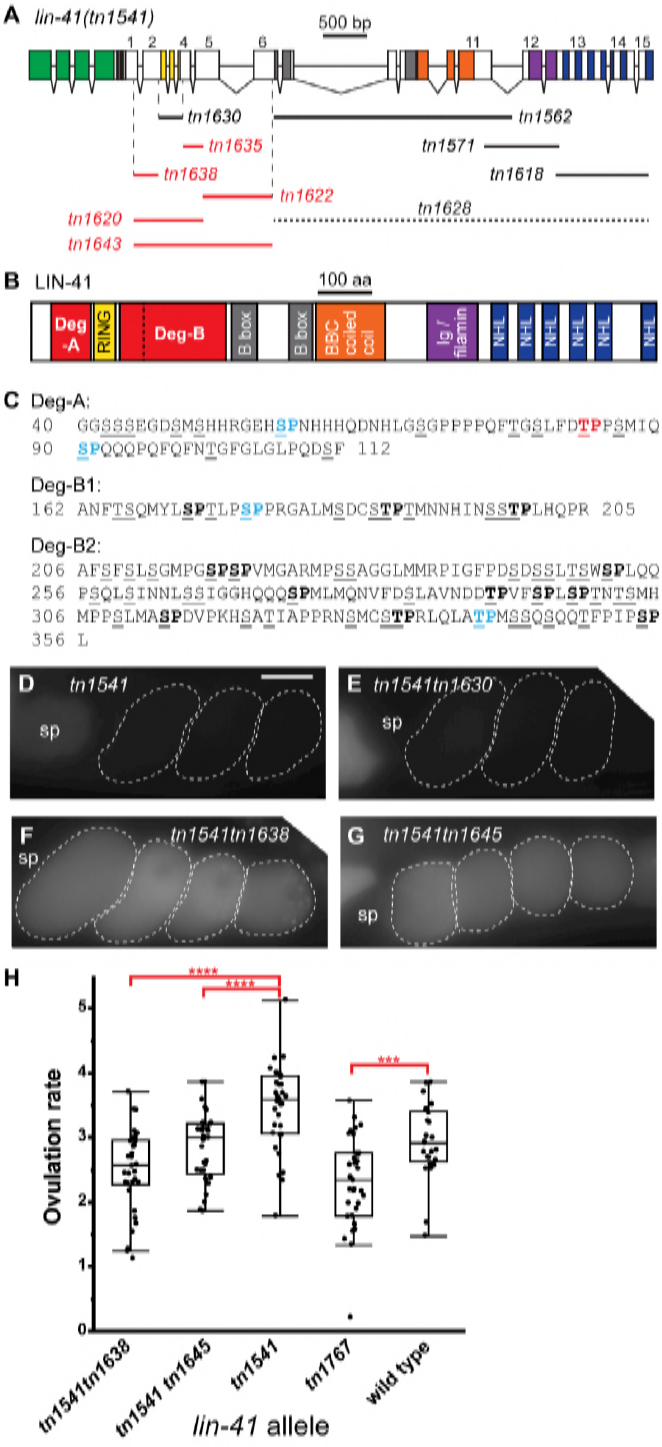

1670

1671 FIGURE 2. GFP::LIN-41 elimination requires two non-overlapping regions of LIN-41 and a

1672 potential phosphorylation site. (A) The exon-intron structure and deletion analysis of *lin-*

41(tn1541). Colored boxes indicate exonic regions that encode GFP (green) or previously described protein domains of LIN-41 (see (B)). Deletions made in the context of *lin-41(tn1541)* are drawn as lines, labeled with a deletion-specific allele name, below LIN-41-encoding exons and introns (exons labeled 1–15). GFP::LIN-41 can be detected in the germline of most deletion mutants (solid lines), with one exception (*tn1628*, dotted line). Deletions in red prevent the elimination of GFP::LIN-41 from early embryos. The vertical dashed lines delimit the beginning of Deg-A and the end of Deg-B, respectively. (B) The previously described (RING (yellow), B-box (gray), BBC (orange), Ig/filamin (purple), NHL (blue)) and newly-identified (Deg (red)) protein domains of LIN-41. The vertical dashed line in (B) indicates the two parts of Deg-B, B1 and B2, which are individually removed in *lin-41(tn1541tn1635)* and *lin-41(tn1541tn1622)*, respectively. (C) The amino acid sequences of Deg-A, Deg-B1 and Deg-B2. Many of the amino acids are serines and threonines (underlined); some are potential targets of proline-directed serine/threonine [S/T] kinases (bold) and have had the [S/T] residue changed to an alanine (colored and bold) in the context of *lin-41(tn1541)*. The T83A mutation in Deg-A results in the persistence of GFP::LIN-41[T83A] in embryos (red), whereas the other changes do not (indicated in blue font). (D–G) GFP::LIN-41 is eliminated from the early embryos (dashed outlines) of *lin-41(tn1541)* (D, control) and *lin-41(tn1541tn1630)* (E, RING deleted) homozygous mutants but persists in the early embryos of *lin-41(tn1541tn1638)* (F, Deg-A deleted) and *lin-41(tn1541tn1645)* (G, LIN-41[T83A]) homozygous mutants. The position of the spermatheca (sp) is indicated, for reference. 100 ms GFP exposures; scale bar, 20 μm. (H) The rate of ovulation is slightly reduced in mutants with a compromised LIN-41 Deg-A domain. Ovulation rate is expressed as the number of ovulations/gonad arm/hour and was measured in at least 25

Day 2 adults. Significance was determined using a Student's *t* test: *P*<.001 is indicated by 3 asterisks, *P*<.0001 is indicated by 4 asterisks. *itIs37[pie-1p::mCherry:::H2B::pie-1 3'UTR, unc-119(+)]* was also present in each of the GFP::LIN-41-expressing strains; it is not expected to alter the ovulation rate.

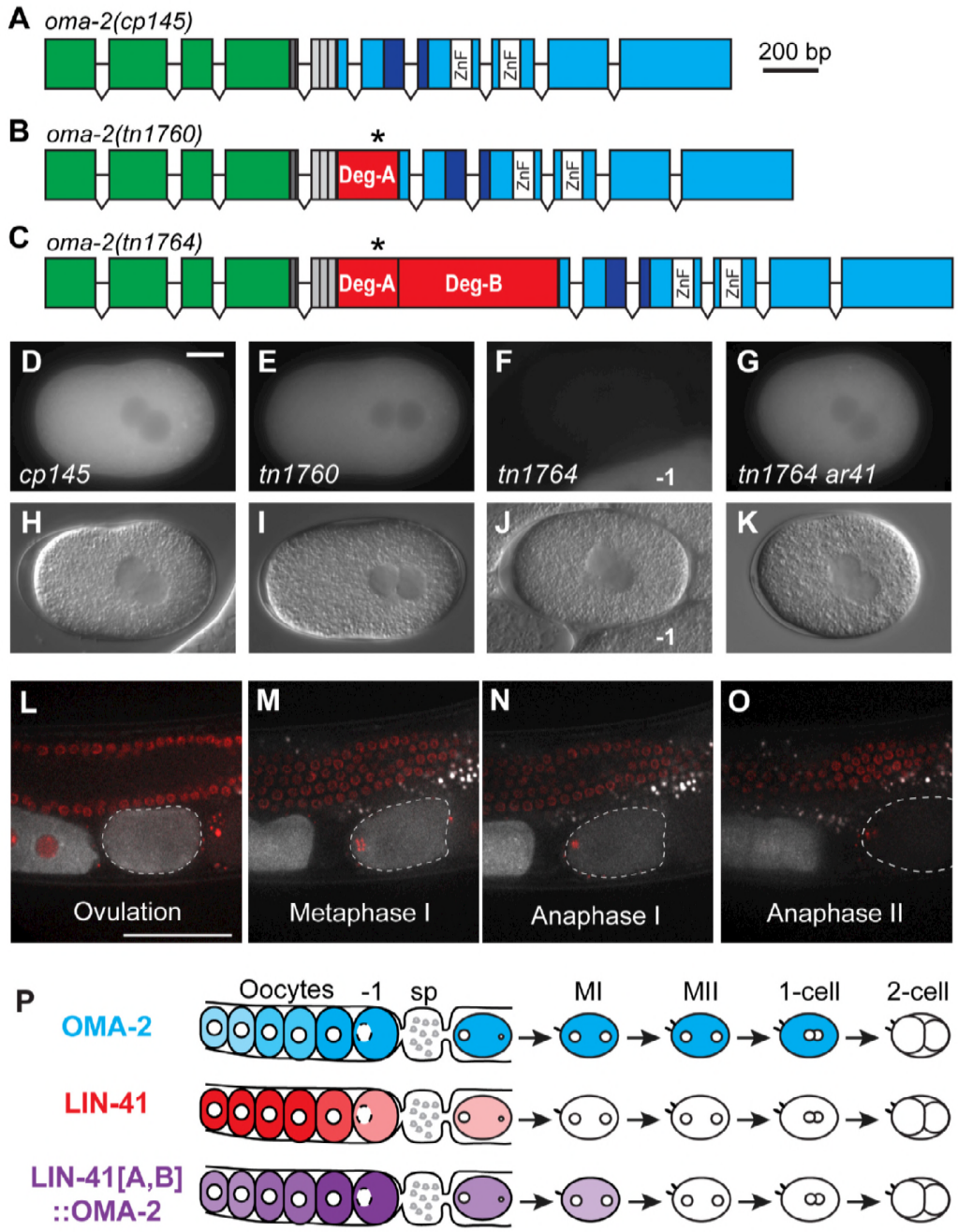

1700

1701 FIGURE 3. LIN-41 degradation domains when implanted into mNG::OMA-2 promote its rapid

1702 elimination during meiosis. (A–C) The exon-intron structures of *oma-*

1703 *2(cp145[mng::tev::3xflag::oma-2]), oma-2(tn1760[mng::tev::3xflag::deg-a::oma-2])* and *oma-*

1704 *2(tn1764[mng::tev::3xflag::deg-a::deg-b::oma-2])*. Boxes represent exonic regions that encode

mNeonGreen (green), the tobacco etch virus cleavage site (TEV, dark gray), FLAG epitope tags (light gray), LIN-41 Deg-A and Deg-B domains (red), the likely TAF-4 interaction domain of OMA-2 (dark blue), two OMA-2 CCCH zinc fingers (white), and other OMA-2 coding sequences (cyan). The position of LIN-41 T83 within the LIN-41 Deg-A domain is indicated by an asterisk. (D–K) GFP (D–G) and DIC (H–K) images of *oma-2(cp145)* (D,H), *oma-2(tn1760)* (E,I), *oma-2(tn1764)* (F, J) and *oma-2(tn1764) lon-3(e2175) sel-10(ar41)* (G, K) 1-cell embryos at pronuclear meeting (E, I), or just slightly later, as the pronuclei begin a counter-clockwise rotation (D, F–G, H, J, and K) prior to NEBD and the first mitotic division. Part of a –1 oocyte is visible in (F, J) and is indicated for reference. 150 ms GFP exposures; scale bar, 10 μm. (L–O) Time-lapse images of mNG::Deg-A,B::OMA-2 (white) and mCHERRY::HISTONE-labeled chromosomes (red) were acquired in a living *oma-2(tn1764); itIs37[pie-1p::mCherry:::H2B::pie-1 3'UTR, unc-119(+)]* adult hermaphrodite by confocal microscopy. Images are shown for select time points (*t*) at ovulation (L, *t*=0 min), during the first (M, *t*=+5 min, N, *t*=+10.5 min) and second meiotic divisions (O, *t*=+24.5 min) as an embryo (dashed outline) progresses through both meiotic divisions. See Movie S3 for the complete time-lapse sequence. Scale bar, 50 μm. (P) A visual summary of the dynamic expression patterns of mNG::OMA-2 (cyan), GFP::LIN-41 (red) and mNG::Deg-A,B::OMA-2 (purple). Oocytes are to the left and embryos are to the right of the spermatheca (sp). Meiotic embryos (MI, MII) have completed their respective divisions.

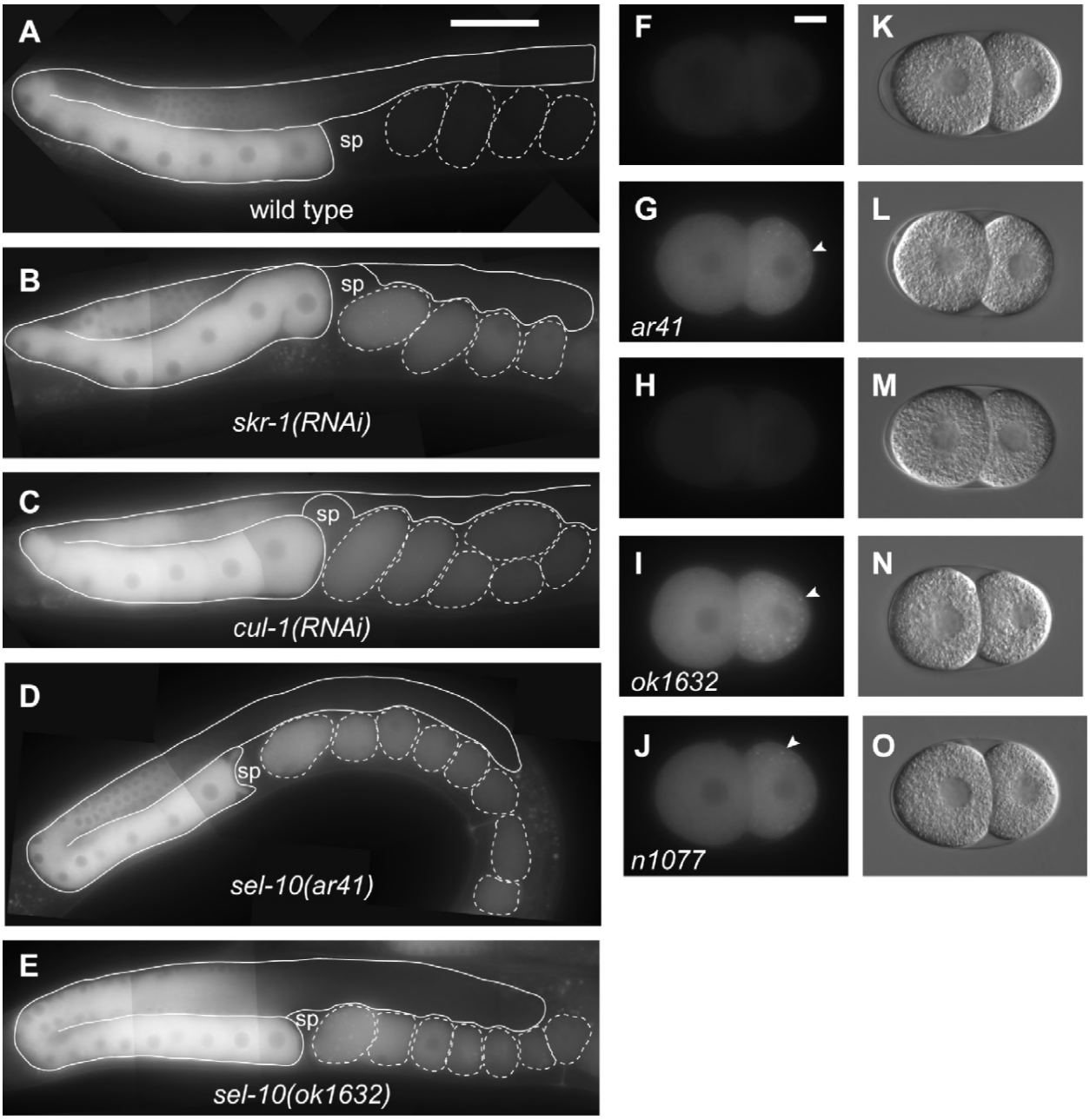

1724

1725 FIGURE 4. Subunits of the SCF^{SEL-10} E3 ubiquitin ligase are required for the elimination of

1726 GFP::LIN-41 from early embryos. (A–E) Composite images of GFP::LIN-41 in adult *rrf-1(pk1417)*

1727 *lin-41(tn1541)* hermaphrodites fed control RNAi bacteria (A), and adult hermaphrodites with

1728 reduced SCF^{SEL-10} E3 ubiqitin ligase activity (B–E): *lin-41(tn1541); skr-1(RNAi)* (B), *rrf-1(pk1417)*

1729 *lin-41(tn1541); cul-1(RNAi)* (C), *lin-41(tn1541); lon-3(e2175) sel-10(ar41)* (D), and *lin-41(tn1541);*

sel-10(ok1632) (E). 100 ms GFP exposures, brightened slightly (and equivalently) to better visualize embryonic GFP::LIN-41; scale bar, 50 μm. (F–O) Images of 2-cell embryos removed from the uterus of hermaphrodites were imaged for GFP (F–J) and DIC (K–O); the genotypes were as follows: *lin-41(tn1541); lon-3(e2175)* (F, K), *lin-41(tn1541); lon-3(e2175) sel-10(ar41)* (G, L), *lin-41(tn1541)* (H, M), *lin-41(tn1541); sel-10(ok1632)* (I,N), and *lin-41(tn1541); sel-10(n1077)* (J, O). Arrowheads indicate a few of the GFP::LIN-41 aggregates in the posterior blastomeres of *sel-10* mutant embryos, which likely correspond to P granules. 300 ms GFP exposures; scale bar, 10 μm.

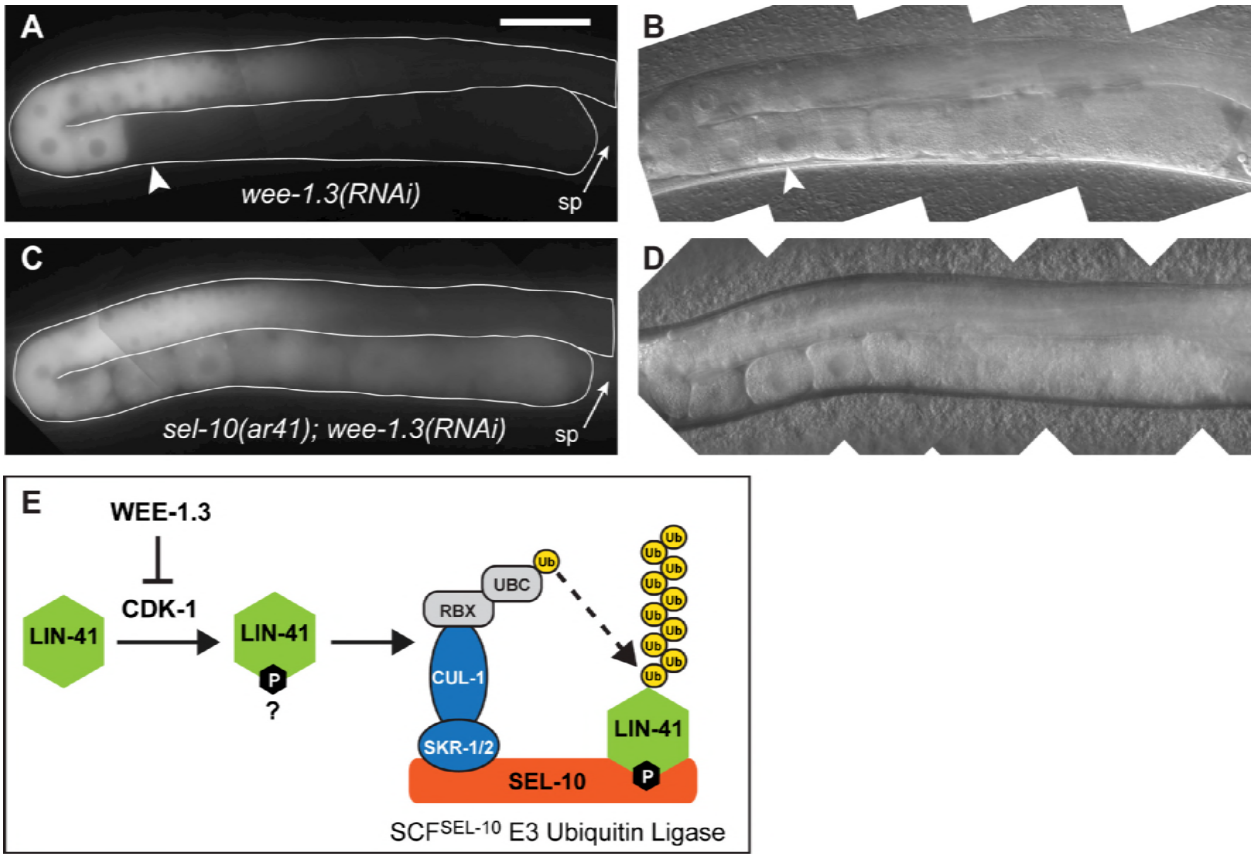

1739

1740 FIGURE 5. SEL-10 is required for the WEE-1.3-inhibited degradation of GFP::LIN-41. (A–D)

1741 Composite GFP (A, C) and DIC (B, D) images of *lin-41(tn1541); lon-3(e2175); wee-1.3(RNAi)* (A,

1742 B) and *lin-41(tn1541); lon-3(e2175) sel-10(ar41); wee-1.3(RNAi)* (C, D) animals. GFP::LIN-41 is

1743 prematurely eliminated from oocytes by *wee-1.3(RNAi)* (arrowhead), but persists in abnormal

1744 oocytes near the spermatheca (sp, arrow) in *sel-10(ar41); wee-1.3(RNAi)* animals (C, D),

1745 suggesting that SEL-10 is required for this process. 150 ms GFP exposures, brightened slightly;

1746 scale bar, 50 μm. (E) A simple model for the elimination of LIN-41 (green) that incorporates the

1747 known molecular functions of WEE-1.3 kinase, cyclin-dependent kinase (CDK-1) and subunits of

1748 the SCF^{SEL-10} E3 ubiquitin ligase. In brief, we hypothesize that SEL-10 (orange) may recognize

1749 phosphorylated LIN-41 (green) and trigger its ubiquitin-mediated degradation in collaboration

with the other SCF E3 ubiquitin ligase subunits, SKR-1/2 (blue) and CUL-1 (blue). CUL-1 orthologs bind RING finger proteins (RBX, gray), which recruit a ubiquitin-conjugating enzyme (UBC, gray) that catalyzes the transfer of ubiquitin (yellow) to protein substrates, such as LIN-41. Subsequent recruitment of poly-ubiquitinated substrates to the proteasome results in degradation (not shown). This model is consistent with the epistatic relationship between *wee-1.3(RNAi)* and *sel-10(ar41)* with respect to the elimination of GFP::LIN-41, but other models are also possible.

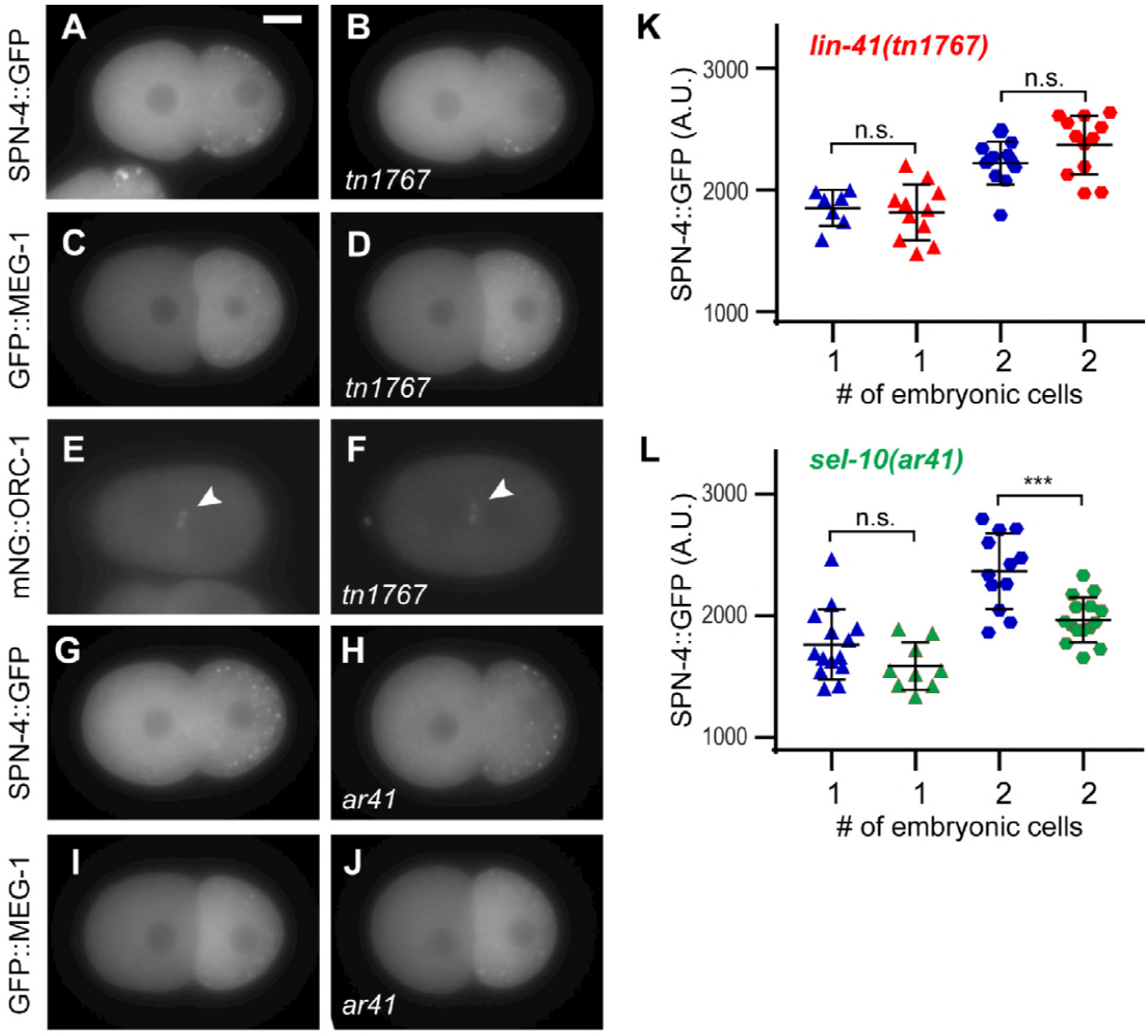

1758

1759 FIGURE 6. Persisting LIN-41 or LIN-41[T83A] does not strongly inhibit the expression of LIN-41

1760 targets of translational repression in young embryos. (A–J) Young embryos express similar

1761 levels of SPN-4::GFP (A, B, G, and H), GFP::MEG-1 (C, D, I, and J) and mNG::ORC-1 (arrowhead in

1762 E, F) when ectopic LIN-41[T83A] (B, D, and F; *lin-41(tn1767)* mutant embryos), ectopic LIN-41

1763 (H, J; *sel-10(ar41)* mutant embryos) or normal (undectable) levels of LIN-41 (B, D, F, H, and J)

1764 are present. Exposures were 100 ms for SPN-4::GFP, 200 ms for GFP::MEG-1 and 600 ms for

1765 mNG::ORC-1; scale bar, 10 μm. (K) Quantification of the intensity of SPN-4::GFP expression in

1766 *spn-4(tn1699)* and *lin-41(tn1767); spn-4(tn1699)* 1 and 2-cell embryos. No significant
1767 differences were seen (n.s.). (L) Quantification of the intensity of SPN-4::GFP expression in *spn-*
1768 *4(tn1699); lon-3(e2175)* and *spn-4(tn1699); lon-3(e2175) sel-10(ar41)* 1 and 2-cell embryos.
1769 Levels appeared to be slightly lower in the *sel-10(ar41)* 2-cell embryos (*P*<.001). Note that the
1770 slightly reduced level of SPN-4::GFP in image (H) relative to image (G) accurately illustrates the
1771 very modest magnitude of this difference in expression.

1772

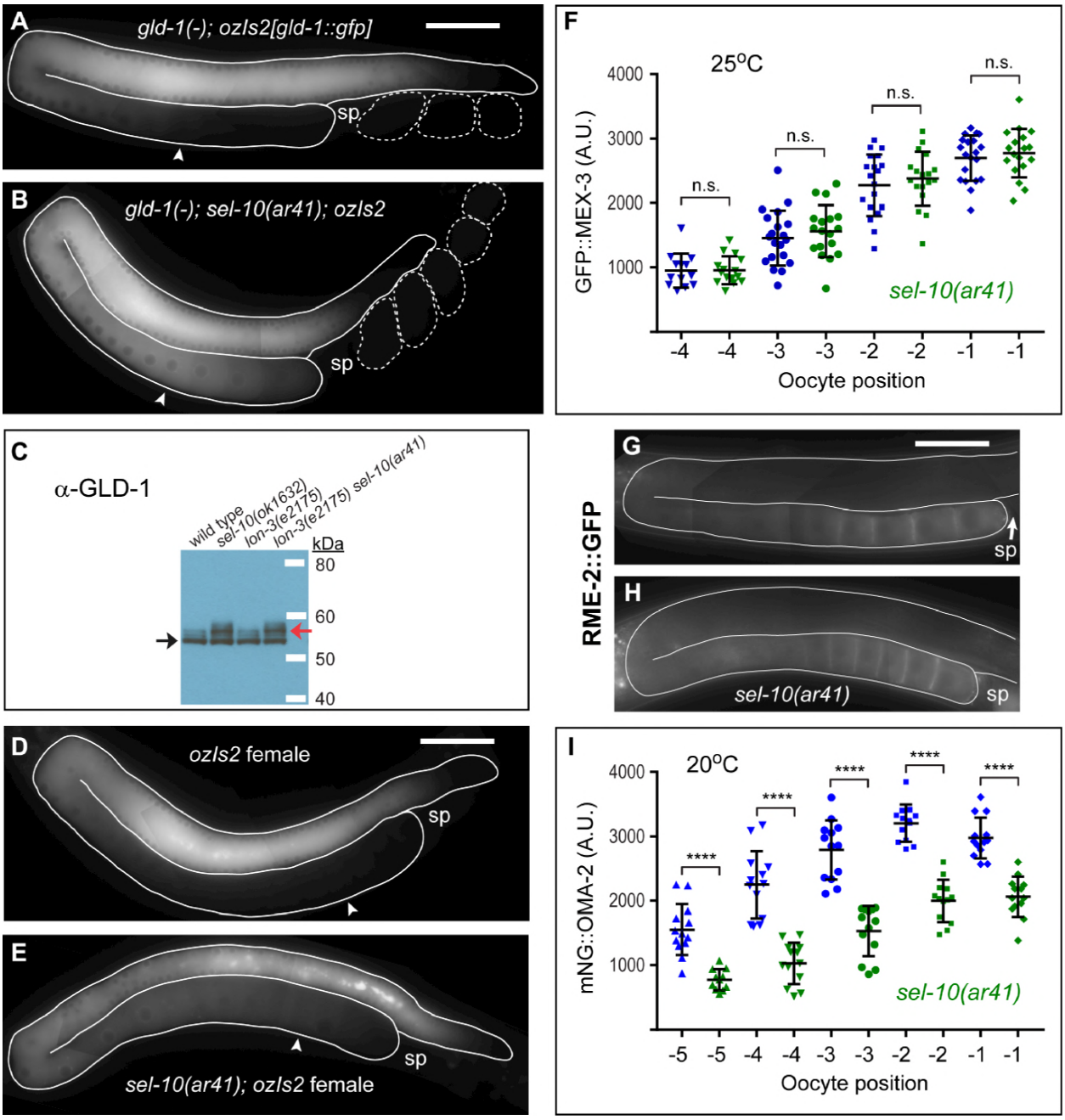

1773

1774 FIGURE 7. GLD-1 persists at elevated levels in the oocytes of *sel-10(ar41)* mutants. (A, B)

1775 Composite images of GLD-1::GFP in *gld-1(q485); lon-3(e2175); ozIs2[gld-1::gfp]* (A) and *gld-*

1776 *1(q485); lon-3(e2175) sel-10(ar41); ozIs2[gld-1::gfp]* (B) adult hermaphrodites. GLD-1::GFP

1777 levels remain elevated in the proximal oocytes (e.g.: –4 oocytes, arrowheads) of *sel-10(ar41)*

1778 animals (B) relative to controls (A). 17 ms GFP exposures, brightened slightly. (C) Slow-migrating

forms of GLD-1 (red arrow) are more abundant in *sel-10(lf)* adult hermaphrodites than in *sel-10(+)* controls, where the fast-migrating form of GLD-1 (black arrow) predominates. (D, E) Composite images of GLD-1::GFP in *fog-3(q470); lon-3(e2175); ozIs2[gld-1::gfp]* (D) and *fog-3(q470); lon-3(e2175) sel-10(ar41); ozIs2[gld-1::gfp]* females (E). GLD-1::GFP levels are elevated in the proximal oocytes (e.g.: –4 oocytes, arrowheads) of *sel-10(ar41)* females (B) relative to controls (A), although this is not as dramatic as in hermaphrodites. A somewhat longer GFP exposure (35 ms, brightened slightly) was needed than in (A and B), likely due to the presence of endogenous GLD-1. (F) Quantification of the intensity of GFP::MEX-3 in the proximal oocytes of *lon-3(e2175); mex-3(tn1753)* and *lon-3(e2175) sel-10(ar41); mex-3(tn1753)* hermaphrodites at 25°C. No significant differences were seen (n.s.). (G-H) Composite images of *lon-3(e2175); pwIs116[rme-2p::rme-2::GFP::rme-2 3'UTR]* (G) and *lon-3(e2175) sel-10(ar41); pwIs116 [rme-2p::rme-2::GFP::rme-2 3'UTR]* (H) hermaphrodites at 22°C. 300 ms GFP exposures. Neither target of GLD-1 translational repression (MEX-3, RME-2) was strongly or even marginally reduced in expression in *sel-10(ar41)* oocytes. (I) Quantification of the intensity of mNG::OMA-2 in the proximal oocytes of *oma-2(cp145) lon-3(e2175)* and *oma-2(cp145) lon-3(e2175) sel-10(ar41)* hermaphrodites at 20°C. Differences in expression were highly significant ($P<.0001$, indicated by 4 asterisks), but relatively modest in magnitude. For example, we measured a 37% reduction in average fluorescence in the –2 oocytes of *sel-10(ar41)* animals relative to the same oocytes in control animals. Scale bar, 50 μm (A, B, D, E, G, and H).